Mid- and End-of-Century Snowfall in the Los Angeles Region

Part II of the "Climate Change in the Los Angeles Region" Project

UCLA Institute of the Environment and Sustainability

LARC
Los Angeles Regional Collaborative for Climate Action and Sustainability

MID- AND END-OF-CENTURY SNOWFALL IN THE LOS ANGELES REGION

Part II of the "Climate Change in the Los Angeles Region" Project

Fengpeng Sun, PhD
Assistant Researcher
UCLA Dept. of Atmospheric and Oceanic Sciences

Alex Hall, PhD
Professor
UCLA Dept. of Atmospheric and Oceanic Sciences

Daniel Walton
Graduate Student
UCLA Dept. of Atmospheric and Oceanic Sciences

Scott Capps, PhD
Assistant Researcher
UCLA Dept. of Atmospheric and Oceanic Sciences

Katharine Davis Reich
Staff Research Associate
UCLA Dept. of Atmospheric and Oceanic Sciences

Funding for this project was provided by the U.S. Department of Energy and the National Science Foundation.

For information, contact:
Professor Alex Hall
UCLA Dep't of Atmospheric and Oceanic Sciences
7955 Math Sciences Building
405 Hilgard Ave., Box 951565, Los Angeles, CA 90095
alexhall@atmos.ucla.edu • www.atmos.ucla.edu/csrl

Electronic copies of this study are available at: www.c-change.la

Table of Contents

Abstract

Using a combination of dynamical and statistical downscaling techniques, we produced 2-km-resolution future projections of snowfall in the Los Angeles region for the mid-21st-century (2041–2060) and end-of-21st-century (2081–2100). Projections from both time periods were compared to a validated simulation of a baseline period (1981–2000) to measure snowfall change. We examined outcomes associated with two emissions scenarios: a "business-as-usual" scenario (RCP8.5) and a "mitigation" scenario (RCP2.6). Output from all available global models in the recently generated CMIP5 archive was downscaled. We found that by mid-century, the mountainous areas in the Los Angeles region are likely to receive substantially less snowfall than in the baseline period. In RCP8.5, 58% of the snowfall is likely to persist, while in RCP2.6, the likely amount remaining is somewhat higher (69%). By end-of-century, however, the two scenarios diverge significantly. In RCP8.5, snowfall sees a dramatic further reduction, with only about a third of baseline snowfall persisting. For RCP2.6, snowfall sees only a negligible further reduction from mid-century. Due to significant differences in climate change outcomes across the global models, these numbers are associated with uncertainty, in the range of 15–30 percentage points. For both scenarios and both time slices, the snowfall loss is consistently greatest at low elevations, and the lower-lying mountain ranges are somewhat more vulnerable to snowfall loss. The similarity in the two scenarios' most likely snowfall outcomes at mid-century illustrates the inevitability of climate change in the coming decades, no matter what mitigation measures are taken. Their stark contrast at century's end reveals that reduction of greenhouse gas emissions will help avoid a dramatic loss of snowfall by the end of the century. In other words, the benefits of climate change mitigation measures do eventually materialize, but decades into the future.

1 Background

1.1 About This Project

The greater Los Angeles area is home to nearly 18.1 million people, who together account for nearly $755 billion in economic activity every year (U.S. Metro Economies – Outlook – Gross Metropolitan Product, and Critical Role of Transportation Infrastructure, 2012). The Los Angeles region has a complex geomorphology and climate system that is highly variable across the landscape, making it difficult to infer local implications of global climate change estimates. It is therefore critical to assess climate change in the region and determine its impacts at space and time scales relevant for municipal planning and policymaking. The "Climate Change in the Los Angeles Region" project is meant to facilitate this assessment activity, and provide a quantitative foundation for a regional action plan in the areas of climate change adaptation and mitigation. The project relies on output from publicly available global climate change simulations. These simulations are state-of-the-art, but because they are global, their resolution (roughly 200 km [124 miles] on average) is too coarse to provide meaningful information about climate change at the regional scales of interest for this project. Therefore, we undertook additional high-resolution simulations to regionalize the climate change signals implicit in current global simulations. This particular study focuses on the changes in snowfall in the greater Los Angeles region. Other critical aspects of climate change in the region, including those related to temperature, precipitation, surface hydrology, and Santa Ana winds, are presented in companion studies. The first study in this project, *Mid-Century Warming in the Los Angeles Region,* was released in June 2012.

1.2 Climate Change and Snow Reduction

Streamflow from mountain snow is one of the critical water resources for California. The natural reservoir that snow provides is important for water supply management and planning. Snowpack may be substantially reduced with climate change due to increases in atmospheric greenhouse gas concentrations. This reduction may occur due to both a conversion of precipitation from snow to rain, resulting in less snowfall, and an acceleration of snowmelt processes, resulting in a shorter residence time of snow on the ground. There have been many studies documenting snowpack changes during the past decades, and assessing impacts of global and regional warming on snowpack (Barnett et al. 2008, Kapnick and Hall 2010). Meanwhile, several observational and numerical modeling studies have investigated the potential effects of projected

warming on the snowpack of the Sierra Nevada (e.g., Howat and Tulaczyk 2005, Mote et al. 2005, Mote 2006, Kapnick and Hall 2010, Pavelsky et al. 2011) and other mountainous regions in the Western United States (Bales et al. 2006, Knowles and Cayan 2002, Kim et al. 2002, Snyder et al. 2004, Kapnick and Hall 2012, Pierce and Cayan 2012). Few studies have focused on snow variability and change in Southern California. Using a combination of dynamical and statistical downscaling techniques to produce high-resolution regional climate reconstructions and projections, this study quantifies the sensitivity of snowfall to temperature in mountain regions surrounding the Los Angeles metropolitan area and projects future snowfall changes in the region at the middle and end of the 21st century. The main subject of this study is the change in the amount of snow falling in the region, rather than the acceleration of snowmelt due to a warming climate. We address the net effect of changes in snowfall and snowmelt on snowpack in the conclusion.

2 The Global Climate Simulations

The global climate model simulations noted above are widely used for understanding and projecting future global climate change resulting from increases in atmospheric concentrations of greenhouse gases and other factors affecting the planet's energy balance. We rely on a recently released data archive of coordinated global climate change experiments, known as the Fifth Coupled Model Intercomparison Project (CMIP5). CMIP5 contains output from dozens of state-of-the-art global climate models ("general circulation models" or GCMs) developed at leading climate research centers around the world. This data set allows the scientific community to address outstanding questions surrounding climate change. It also forms the basis of the forthcoming Fifth Assessment Report (AR5) of the United Nations Intergovernmental Panel on Climate Change (IPCC). CMIP5 provides a multi-model context for understanding the relationship between factors affecting the planet's energy balance and climate change. It also provides a range of climate responses across the different GCMs under multiple greenhouse gas emissions scenarios (Taylor et al. 2009).

A set of future emissions scenarios known as Representative Concentration Pathways (RCPs) has been adopted by the organizers of the CMIP5 archive (Moss et al. 2008, Meinshausen et al. 2011). Four RCPs have been developed: RCP2.6, RCP4.5, RCP6, and RCP8.5. The names of the scenarios correspond to the approximate radiative forcing (the globally averaged change to the planet's energy balance) they would produce at the end of the

21st century (2.6, 4.5, 6.0, and 8.5 watts per square meter [W/m^2], respectively). The radiative forcing up to the year 2100 is shown in Fig. 1a for each scenario, with the historical forcing also shown up to the year 2005. RCP2.6 is representative of a "mitigation" scenario in which greenhouse gas emissions peak roughly within the next two decades and then decline steadily. The resulting carbon dioxide (CO_2) equivalent concentrations, encompassing the net effect of all anthropogenic forcing agents,[1] reach a maximum level of approximately 460 parts per million by volume (ppmv) around 2050 and decline thereafter to approximately 420 ppmv by 2100 (Fig. 1b). Total radiative forcing relative to pre-industrial levels peaks at about 3 W/m^2 in the middle of the 21st century and declines to 2.6 W/m^2 by 2100. In contrast to RCP2.6, RCP8.5 represents a "business as usual" scenario, in which greenhouse gas emissions continue to increase throughout the 21st century. The result is a total radiative forcing of 8.5 W/m^2 and CO_2-equivalent concentrations greater than 1200 ppmv by 2100. While RCP8.5 is the most aggressive emissions scenario, it corresponds most closely with emission trends over the past decade. Between the "mitigation" scenario of RCP2.6 and the "business as usual" scenario of RCP8.5 are two "stabilization" scenarios, RCP4.5 and RCP6. In this study, however, we focus on the climate response to the two scenarios at either extreme, i.e., RCP8.5 and RCP2.6, to approximately sample the full range of climate outcomes associated with potential future emissions, without having to downscale output (or show results) from all four emissions scenarios.

The response of global-mean surface air temperature to the RCP2.6 and RCP8.5 scenarios seen in the CMIP5 GCMs is shown in Fig. 1c. (Table 1 summarizes the available global climate models used in this study from the CMIP5 archive.) For both scenarios, there are clearly significant model-to-model differences in the warming response over the course of the 21st century. The variations arise principally from differences in the GCMs' spatial resolutions and physical parameterizations. The resolution of GCMs varies, ranging from ~100 to ~300 km. These parameterizations are formulated at the various modeling centers, and they represent processes occurring at scales smaller than the GCM grid scale, especially those associated with cloud cover, the atmospheric boundary layer schemes, and oceanic eddies. Thus the set of lines for each scenario seen in Fig. 1c approximately represent the range of warming outcomes associated with the various ways of constructing a physically-based climate model. For this reason, we interpret the range of outcomes as the climate change uncertainty associated with a given emissions scenario. We also interpret the average response of all the GCMs for a given

[1] Anthropogenic factors that influence radiative forcing include changes in greenhouse gas concentrations, aerosols, ozone, and land use (e.g., deforestation).

emissions scenario (the “ensemble mean”) as the most likely outcome for that scenario. This assumes the GCMs randomly sample the uncertainty space associated with the simulated response to anthropogenic forcing. This is the same approach to likelihood and climate change uncertainty quantification used in previous IPCC reports (Meehl et al. 2007) and to be used by the IPCC-AR5.

We focus on three time periods in this study: a “baseline” (1981–2000), a "mid-century" (2041–2060), and an "end-of-century" (2081–2100). These three periods are shaded in Fig. 1. Climate change is quantified by comparing the mid-century and end-of-century climate states with the baseline climate state. At mid-century, the least sensitive GCMs show about as much warming under the RCP8.5 scenario as the most sensitive ones under RCP2.6 (see Fig. 1c), and thus there is an overlap in the two scenarios' uncertainty ranges. It is not until the latter third of the century that the range of simulated climate change associated with RCP8.5 becomes entirely distinct from that associated with RCP2.6. In Part I of this project, which assessed temperature changes in the Los Angeles region, we focused on the mid-century time period because it is far enough in the future to allow for unambiguous climate change signals but still within a time horizon pertinent to the interests of policymakers and local stakeholders. When we downscaled the GCMs to the Los Angeles region, we found the two scenarios behave the same way locally as they do globally, with a large overlap in their uncertainty ranges. In this study, we add the end-of-century time period because this is where we expect regional climate outcomes associated with RCP 8.5 and RCP2.6 to diverge. Assessing the differences will allow policymakers and the public to evaluate outcomes with and without global mitigation efforts and understand the longer-term implications of each scenario. As a frame of reference: a child born today in the United States with an average life expectancy will live to experience this end-of-century climate.

3 The Need for Dynamical and Statistical Downscaling

The typical resolution of current GCMs (~200 km, see Table 1) is too coarse to accurately characterize climate variability and change at a local scale in the Los Angeles region, with complex topography and meandering coastlines. GCMs calculate climate over a patchwork of grid cells that blanket the globe. The resolution of a climate model refers to the length of a side of each grid cell. A 200-km-resolution GCM thus produces climate output that is averaged over grid cells of 40,000 km^2. This leads to the smoothing and leveling of mountains and reduction of meandering coastlines to straight lines. Because of their relatively coarse resolution, GCMs

simulate regional-scale climate dynamics poorly, including local circulations shaped by topography, land-sea breezes and mountain/valley circulation systems, and orographic precipitation. The topography is the surface shape and features of terrains. The local topography plays an important role in shaping the local circulation and climate. For example, the orographic precipitation is generated mainly by a forced upward movement of the moist air upon encountering a mountain. All of these phenomena have significant manifestations in the Los Angeles region. Indeed, previous studies have confirmed that taking into account climate processes with spatial scales of a few km is important for simulating and understanding current climate variability in the region and in the rest of the state of California (e.g., Cayan 1996, Conil and Hall 2006, Hughes et al. 2007, Lundquist and Cayan 2007, Cayan et al. 2008, Hughes et al. 2009).

To obtain reliable climate change information at the regional scale, we employ both dynamical and statistical techniques to downscale the relatively coarse-resolution climate information from GCMs to much finer spatial scales. "Dynamical downscaling" refers to the use of regional numerical models to solve the equations of the atmosphere (and, in some cases, the ocean) over a limited area at high resolution, typically a few to tens of km. Apart from their regional focus and higher resolution, these models are very similar to GCMs. The regional models are typically driven by coarse-resolution GCM output or reanalysis data along the boundaries. This allows for simulations of fine-scale physical processes that are consistent with the atmospheric evolution encoded in the larger-scale data product. Dynamical downscaling has been widely applied over many regions to examine a range of climate change impacts (Leung and Ghan 1999, Giorgi et al. 2001, Wang et al. 2004, Chin 2008). This approach has already proven valuable in providing information on California climate change, including impacts on temperature, snowpack, and the hydrologic cycle (Leung et al. 2003, Cayan et al. 2008, Caldwell et al. 2009, Qian et al. 2010, Pan et al. 2011). The other downscaling technique we use—statistical downscaling—relies on empirical mathematical relationships between known climate predictors and climate variables of interest at the regional scale. These relationships are then used to project regional climate change given the change in the climate predictors (von Storch et al. 1993, Wilby et al. 2004).

The main advantage of dynamical downscaling is that the regional numerical model produces a climate change response driven purely by its own internal dynamics and the provided boundary conditions. Unlike a climate response produced by statistical downscaling, a dynamically downscaled response is not predetermined by any assumptions about the

relationship between regional climate and climate at larger scales. However, this benefit of dynamical downscaling must be balanced against its very high computational cost. Generally, a regional climate change simulation will require several months of computer time. Since it is highly impractical to dynamically downscale every global climate model forced by each emissions scenario, it is nearly impossible to fully characterize climate change uncertainty with dynamical techniques alone. For this reason, we employed statistical techniques, which have the advantage of negligible computational costs, in conjunction with dynamical downscaling. The basic idea was to undertake dynamical downscaling for a small representative sample of GCMs forced by a single emissions scenario (RCP8.5) for the mid-century time slice. Then we developed a statistical model that projects regional snowfall change independently of those simulations. We proved the statistical model is accurate by comparing its predictions to those of the dynamical downscaling simulations. Finally, we applied the remaining GCMs' parameters to the validated statistical model to project regional snowfall change for the remaining GCMs without dynamical downscaling. The statistical model could also be applied to project snowfall for other time slices and other emissions scenarios.

Combining dynamical and statistical downscaling techniques in this way allows us to incorporate the most important dynamical processes shaping regional snowfall change and quantify most likely outcomes and approximate uncertainties associated with the various global climate projections and the two emissions scenarios.

4 Dynamical Downscaling Methods

4.1 Simulations

To perform the dynamical downscaling, we used the Weather Research and Forecasting Model (WRF; Skamarock et al., 2008) version 3.2. For details on WRF and the dynamical downscaling technique, the reader is referred to Part I of the "Climate Change in Los Angeles Region" project (Hall et al., 2012). Fig. 2 shows a blow-up of the topography and coastlines for the innermost domain of the WRF configuration we used, covering the Los Angeles region, at its native 2-km resolution. The main features of both the topography and coastlines are represented well at this resolution.

Using this model configuration, we performed a “baseline” simulation whose purpose is two-fold: (1) to validate the model’s ability to simulate regional climate (in this case, snowfall distributions), and (2) to provide a baseline climate state against which future climate simulations

could be compared. This simulation is a dynamical downscaling of a publicly available, 32-km resolution data archive of the weather and climate variations over North America during the baseline period (1981–2000). The simulation is designed to reconstruct, at 2-km resolution, the actual regional weather and climate variations that occurred during this time period, and its output can be compared with available observations for model validation purposes. The coarse-resolution archive used to force the regional model is the National Centers for Environmental Prediction 3-hourly North America Regional Reanalysis (NARR) data. This dataset provides lateral boundary conditions at the outer boundaries of the outermost domain (see Fig. 2 in our Part I study). It also provides surface boundary conditions over the ocean (i.e., sea surface temperature).

Using the same model configuration, we also performed a series of dynamical downscaling experiments whose purpose is to simulate regional climate states associated with five GCM simulations during the mid-century period (2041–2060). The output of these experiments can be compared with the baseline simulation to measure simulated regional climate change. The global models we chose are NCAR Community Climate System Model version 4 (CCSM4; Gent et al. 2011), the NOAA Geophysical Fluid Dynamics Laboratory Climate Model 3 (GFDL-CM3; Donner et al. 2012), the Centre National de Recherches Meteorologiques Climate Model 5 (CNRM-CM5, Voldoire et al. 2012), the AORI (U. Tokyo), NIES, and JAMSTEC Atmospheric Chemistry Coupled MIROC Earth System Model (MIROC-ESM-CHEM; Watanabe et al., 2011), and Max Planck Institute for Meteorology Low Resolution Earth System Model (MPI-ESM-LR; Brovkin et al.). As shown in our Part I temperature study, the warming response in CNRM-CM5 is similar to CCSM4, showing lower sensitivity to greenhouse gas emissions (i.e., less warming). GFDL-CM3 and MIROC-ESM-CHEM show higher sensitivity (i.e., more warming), whereas MPI-ESM-LR shows moderate sensitivity. In terms of their warming, these models very roughly span the full CMIP5 ensemble.

To produce future climate boundary conditions for the regional model, we quantified the differences in GCM monthly climatology between the mid-century and baseline periods. These differences are the climate change signals of interest that develop in the GCM simulation. All variables were included in this calculation of the climate change signal (i.e., 3-dimensional atmospheric variables such as temperature, relative humidity, zonal and meridional winds, and geopotential height and 2-dimensional surface variables such as temperature, relative humidity, winds and pressure). On a monthly varying basis, we added these climate change signals to the NARR reanalysis data corresponding to the baseline period. Thus, we perturbed the NARR

baseline data with climate change signals provided by the GCM. This technique has been used to downscale global warming signals to regional scales at other regions (e.g., Sato et al., 2007, Hara et al., 2008, Kawase et al., 2009 and Rasmussen et al., 2011). We used this perturbed NARR data to construct the boundary conditions imposed on the outermost domain of the regional model. The resulting simulation could then be compared directly with the baseline regional simulation to assess the impact of the GCM climate change signals when they are downscaled. CO_2 levels were also increased in WRF to match the changes in CO_2-equivalent radiative forcing in the RCP8.5 scenario averaged over the mid-century period compared to the baseline.

Fig. 3 presents the baseline dynamically downscaled spatial distributions of snowfall over the Los Angeles region for the region's wet months (November to April). The values are the climatological means over the entire baseline period (1981–2000). January, February, and March see the largest snowfall for most areas and have the largest spatial extent of snowfall. These three months account for more than half of the annual snowfall across the region. Snowfall is mainly found in mountain regions, at elevations of 4000 feet and higher (see Fig. 3). It generally follows the topography, increasing with elevation, with larger amounts on the coastward-facing side of the ranges. Note that in high-elevation desert regions (e.g., the Mojave Desert), some snowfall is simulated, but the climatological value is negligible, less than 0.5 inches per month (not shown in colorbar). Such a tiny amount of snow would probably not survive long enough on the ground to lead to any substantial accumulation, especially when the surface air temperature is not cold enough. Snowfall greater than 10 inches per month is seen in high-elevation mountain regions (6000 feet and higher), including the southern rim of the Sierra Nevada Mountains and the Tehachapi, San Emigdio, San Gabriel, San Bernardino, and San Jacinto Mountains. At the peaks of the mountain ranges, monthly accumulated snowfall can reach more than 40 inches per month in January, February, and March.

4.2 Validation of the Baseline Snowfall Simulation

In this section, we validate the dynamical model's capacity to reproduce the snowfall climatology and its temporal and spatial variations. We do this by comparing the 2-km high-resolution baseline simulation with *in-situ* snowfall measurements. The observational data were obtained from the Western Regional Climate Center (WRCC), which collects monthly climate data from the National Weather Service (NWS) Cooperative Observer Program (COOP). The NWS-COOP is the United States' weather and climate observing network, consisting of more

than 11,000 sites run by well-trained and organized volunteers taking climate observations in urban and suburban areas and National Parks and on farms, seashores, and mountaintops. These data have been processed by WRCC and quality-controlled.

We evaluated the data from each NWS-COOP station within the 2-km WRF domain. At most stations, no snowfall has been recorded, so these locations were excluded. We selected from the remaining stations on the basis of several criteria. First, the station must have snowfall data available for a period covering at least 75% of the baseline period. Second, the number of days in each month with missing data should not be greater than 5 days. Finally, the sites should be representative of the distribution of mountain regions within our 2-km WRF domain. Four stations met these criteria: Big Bear Lake and Lake Arrowhead in the San Bernardino Mountains, Idyllwild in the San Jacinto Mountains, and Tehachapi in the Tehachapi Mountains. Table 2 summarizes the identifying information associated with each observational station, including COOP ID, location, elevation, and period of available data. All four stations are in mountain regions, varying in elevation and in the length and completeness of the observational snowfall record. The first three stations have records covering the whole baseline period. Tehachapi's records cover only the first 16 years, but that is long enough for both climatology and interannual variability assessment. At these four stations, individual months are not used for monthly statistics if more than 5 days are missing, and individual years are not used for annual statistics if any month in that year has more than 5 days missing.

Aside from missing data, there are factors affecting the quality of the observations. Snowfall is usually measured with a gauge that collects fallen snow; resulting accumulations are measured periodically. Snow gauges should be shielded from wind exposure so that wind does not blow snow away from the gauge or into the gauge from other locations. In practice, some snow gauges are not shielded. If measurements are reported from areas with open exposure to strong winds or from time periods with strong winds, it is very difficult to relate them to the original snow that fell at the measurement site (Pomeroy and Brun 2001, Meyer et al., 2012). It is possible that the observed snowfall data we use could be contaminated by wind blowing and drifting. The quality of observational snowfall data also depends on the inherent accuracy of the measurement, and proper recording of the measurement timing (Judson and Doesken 2000).

There are two respects in which it is not straightforward to compare observed and simulated snowpack data. First, the model grid cells in the vicinity of a measurement station may not be at the exact elevation as the measurement station. Because of the strong dependence of snowfall on elevation, this can lead to a slight artificial mismatch between observed and

simulated data. To minimize this issue, of the five model grid cells nearest each station, we selected the model grid cell whose elevation is in closest agreement with that of the station for validation. Second, the model produces snowfall in terms of snow liquid water equivalent. For comparison to observations, this value must be converted to snow depth by assuming a density of freshly fallen snow. Unfortunately this number is not measured, and so we are forced to assume it is constant. In reality, it varies widely by location, meteorological condition, crystal size, crystal shape, degree of riming, and other snow metamorphosis processes, from 10 to 500 kg/m^3 (e.g., Judson and Doesken, 2000; Pomeroy and Brun 2001, Roebber et al. 2003, Baxter et al. 2005, Kay 2006). The most common values are between 60 and 100 kg/m^3 (Judson and Doesken 2000). In this study, we use the value suggested by Baxter et al. (2005): 80 kg/m^3. These two inherent barriers to straightforward comparison of observed and simulated data, together with the substantial observational data quality issues noted above, mean that disagreement between observed and simulated snowfall is not necessarily an indication of an unrealistic simulation.

With these difficulties in the background we present validation results, focusing on the climatological seasonal cycle and interannual variability. Fig. 4a compares monthly climatological snowfall for observational sites with that simulated by the model. Examining one location at a time (i.e., circles of the same color), it is clear that the model's seasonal cycle of snowfall is consistent with the observations for each location. For each station, the simulated and observed values are extremely well-correlated, with an average correlation of 0.95. In addition, the model also accurately simulates the spatial variations in climatological snowfall. This can be seen by examining the wet months (i.e., the larger snowfall values for each location). The simulated climatological snowfall values track their observed counterparts across the region closely. For example, in both model and observations, Big Bear Lake shows the greatest snowfall, followed by Idyllwild, Lake Arrowhead, and Tehachapi. Overall, Fig. 4a demonstrates that the model reproduces the climatological variations in snowfall in space and across the seasonal cycle extremely well. The overall correlation of the data points in Fig. 4a, providing a combined validation of the model's climatological seasonal and spatial snowfall variations, is greater than 0.96.

Fig. 4b is similar to Fig. 4a, showing interannual snowfall variability instead of monthly snowfall. It compares the annual accumulated (from September to August the following year) simulated snowfall to observations for each location for all years in the baseline period with available data. The year-to-year observed snowfall variations at each location are reasonably well captured by the model simulation. For each station, the simulated and observed values are

significantly correlated, with an average correlation of 0.58. The overall correlation of the data points in Fig. 4b is 0.82, providing a combined validation of the spatial and interannual snowfall variability. The fact that this number is higher than the correlations associated with any individual location is an indication that the model captures spatial variability somewhat better than temporal variability.

Fig. 4 shows that the dynamical model simulates the temporal and spatial variations in baseline snowfall with reasonable accuracy at specific mountain locations where reliable observational data are available. It is likely the agreement would be even better were it not for the inherent difficulties in comparing observed and simulated snowfall data, and the observational data quality issues noted above. Based on this evidence, it is very likely that the model is able to reproduce the temporal and spatial snowfall variations across the whole domain, even in very high mountain regions where there is substantial snowfall but observations are sparse or unavailable.

5 Statistical Downscaling Methods

5.1 Development of a Statistical Model

As noted in Section 3, developing a statistical model allows us to downscale the remaining GCMs, and other scenarios, and other time periods of interest much more efficiently than dynamical downscaling. In this case, the statistical model is built on the mathematical relationships between snowfall and cold extremes in the dynamically downscaled baseline simulation. We applied linear regression analysis to baseline simulated snowfall and temperature on the coldest day of the month to estimate the sensitivity of snowfall to cold extremes. Then we combined this sensitivity with temperature projections from Part I of this project to produce snowfall projections for the future. This concept of sensitivity of snowfall to minimum temperature can be expressed in the following equation:

$$S = \frac{dS}{dT_{min}} T_{min} + B$$

Here dS/dT_{min} is the sensitivity of snowfall to minimum temperature. S is accumulated snowfall for each month, T_{min} is the minimum monthly surface air temperature, defined as the lowest daily-mean temperature of each month, and B is the intercept.

We expect the sensitivity of snowfall to temperature to vary by elevation and season. To determine dS/dT_{min} for each elevation and month, we first binned all the elevations in 250-foot

increments. Then, for all the grid cells lying in each bin, we averaged the snowfall for each month. Similar to snowfall calculation, we also averaged the surface air temperature corresponding to the coldest day of the month over the same area. Thus we obtained year-to-year time series for snowfall and minimum temperature for each month and elevation bin. We then constructed a best-fit linear regression model for each month and elevation. Fig. 5 shows scatter plots of the averaged snowfall values against minimum surface air temperature in a sample elevation bin (5750–6000 feet) for each wet month. The best-fit regression lines are also presented. The fit of the regression for each month is very good (correlation coefficients [r] range from -0.61 to -0.84). Thus, minimum temperature is a powerful predictor of snowfall in the baseline climate, which bodes well for our use of this variable to predict future snowfall knowing temperature alone. The slopes of the regression lines yield a sensitivity of snowfall change for a 1°F T_{min} anomaly. For example, in February, every 1°F increase in T_{min} is associated with a 1.00-inch/month reduction in snowfall, whereas in March, the sensitivity is as high as 1.70 inches/month of reduction per 1 □F increase. This illustrates the seasonally varying nature of the snowfall sensitivity parameter.

To produce a future snowfall projection for a particular grid cell, a particular month, and a particular GCM, we multiplied the snowfall sensitivity parameter for that particular grid cell and that particular month by the change in minimum surface air temperature for that particular month:

$$\Delta S = \frac{dS}{dT_{min}} \Delta T_{min}$$

We calculated ΔT_{min} from the warming projections presented in Part I of our project. Note that for the purposes of this calculation, we assumed that T_{min} increases by the same amount as the monthly mean temperatures provided in the Part I study.

5.2 Validation of the Statistical Model

In this section, we validate the statistical model by comparing its predictions of future snowfall change against those of the dynamical downscaling experiments. We first present the performance of the statistical model in projecting the future change in the full seasonal cycle of snowfall for a single downscaled GCM: CCSM4. Then we present validation results for the other dynamically downscaled GCMs, but to be concise, we do so for annual accumulated snowfall only.

Fig. 6 shows the statistically downscaled mid-21st-century seasonal cycles of snowfall under the RCP8.5 scenario and the corresponding dynamically downscaled results for CCSM4. Data are shown for 4000 (3750–4000 feet bin), 6000 (5750–6000 feet bin), and 8000 (7750–8000 feet bin) feet to represent low, middle, and high elevations within the domain. Examining first the dynamically downscaled results (red lines), there are clearly significant snowfall reductions relative to the baseline in all the elevations through all the wet months. Comparing the red and blue lines, the statistical model reproduces the dynamical model's changes in the snowfall seasonal cycle at all three elevations with an error of only a few percent for nearly all the months.

Fig. 7 shows a comparison of statistically and dynamically downscaled results for annual accumulation, for all five dynamically downscaled models. We first binned all elevations in 250-foot increments, and then calculated the average of annual accumulated snowfall (from September to August of the next year) for each elevation bin. The statistical model tracks the dynamical downscaling results to within a few percent at most elevations (blue and red lines). A comparison of the dynamically and statistically based estimates of snowfall loss (i.e., the difference between the black and red, and black and blue lines) shows that the dynamically predicted snowfall loss is generally captured to within 5–10% by the statistical model. Fig. 7 demonstrates that the statistical model accurately predicts future snowfall loss seen in the dynamically downscaled simulations at all elevations. This gives us confidence that we can use the statistical model, along with the temperature change projections from our Part I study, to project snowfall change for the other GCMs, for both emissions scenarios, and for the end-of-century time slice.

As discussed in Section 5.1, the statistical model is based purely on a sensitivity of snowfall to minimum temperature. However, snowfall ought to be sensitive to precipitation variations as well, and precipitation does change in all five future dynamical downscaling simulations. In Appendix I, we confirm that the change in temperature, rather than precipitation, is by far the dominant control on simulated future snowfall changes.

6 Results

As shown in Fig. 1, all GCMs show significant global warming between mid-century and end-of-century time periods in the RCP 8.5 scenario, and the range of global warming outcomes associated with RCP8.5 becomes entirely distinct from that associated with RCP2.6 toward the end of the 21st century. Under the RCP2.6 scenario, on the other hand, surface warming is stabilized at the end of the century, and there is even a slight cooling compared with mid-century in some GCMs. In this section, we assess local snowfall changes associated with these very different global climate trajectories in the mid-century and end-of-century periods for both emissions scenarios.

As a starting point for the discussion, Fig. 8a shows spatial distributions of annual accumulated snowfall in the baseline simulation. As expected, the spatial pattern is similar to the monthly distributions seen in Fig. 3. Snowfall is mainly found in mid- to high-elevation mountain regions within the domain. It generally follows the topography, with more snowfall at higher elevations. The peaks of the San Bernardino Mountains receive the most snowfall.

6.1 Spatial Patterns of Snowfall Changes

For mid-century under the RCP8.5 scenario, the projected annual accumulated snowfall averaged over all the 18 statistically downscaled regional patterns (ensemble-mean), is shown in Fig. 8b. Compared with Fig. 8a, snowfall is reduced about 40% everywhere within the mountain areas (see also Table 3, which provides spatial averages of the data presented in Fig. 8). Areas of particularly noticeable loss include the northern hills of the San Gabriel Mountains and the areas between the San Gabriel and Tehachapi Mountains. (Enlarged images depicting baseline, mid-century, and end-of-century snowfall under both emissions scenarios in four different sub-domains [the San Emigdio/Tehachapi, San Gabriel, San Bernardino and San Jacinto Mountains] can be found in Appendix II.) Fig. 8c shows the ensemble-mean snowfall distribution under the RCP2.6 scenario at mid-century. The spatial pattern is similar to that of RCP8.5. But the snowfall loss is generally about 30%, less than in RCP8.5. This difference is roughly consistent with the warming difference found between the two scenarios. (See Part I of our project.)

Figs. 8d and 8e present projected snowfall at end-of-century for both emissions scenarios. For the RCP8.5 scenario (Fig. 8d), there is a large continued reduction in both the quantity of snowfall and the area receiving snowfall by the end-of-century. On average, only about one-third of the snowfall occurring in the baseline is also seen at century's end. The area receiving snow in

the San Gabriel Mountains is only about half of the area seen in the baseline simulation. For the San Emigdio and Tehachapi Mountains, similar shrinking of areas receiving snow is also evident. In contrast to the RCP 8.5 scenario, snowfall at the end-of-century under the RCP2.6 scenario (Fig. 8e) is very similar to that at mid-century (Fig. 8c), with an average reduction of just over 30% compared to baseline. Thus further snowfall reduction beyond what occurs by mid-century would be mostly prevented under the mitigation scenario. These results are consistent with the comparison of global warming outcomes between the two periods.

6.2 Sensitivity to Elevation

In Fig. 8, snowfall reductions seem to be more visible at lower elevations. This makes physical sense, since lower elevations start out warmer in the baseline climate, and air temperatures during precipitation events are more likely to breach the freezing point of water as the climate warms. Hence a snow event is more likely to be converted to a rain event at lower elevations. We quantify the snowfall changes as a function of elevation in Fig. 9. This figure shows the future remaining snowfall, calculated as the percentage of the baseline snowfall for three elevations roughly spanning the elevation range affected by snow in the region, 4000, 6000, and 8000 feet. By presenting projections across all GCMs, this figure also gives a sense of the variety of regional snowfall outcomes implicit in the GCM ensemble.

Fig. 9a displays the remaining snowfall in the mid-century under the RCP8.5 scenario for each GCM uniformly at all elevations. The horizontal lines show the ensemble-mean across all the GCMs corresponding to the three elevations. The lowest elevation has the least remaining snowfall, retaining on average only 45% of baseline. The mid- and high-elevation regions are indeed somewhat less sensitive to warming, retaining about 60% of baseline snowfall. It is also evident that each GCM exhibits distinct responses of snowfall to warming. For low-elevation regions, mid-century snowfall is less than 30% of baseline snowfall in the GCM showing the most change, whereas in the GCM showing the least change, mid-century snowfall is nearly 70% of baseline. Fig. 9b shows projections for the RCP2.6 scenario in mid-century. More snowfall remains than in the RCP8.5 scenario (Fig. 9a) at all elevations, consistent with in Fig. 8.

Also consistent with Fig. 8, the end-of-century projections (Figs. 9c and 9d) show a great deal of contrast between the two scenarios. In the RCP8.5 scenario a dramatic snowfall reduction occurs compared with the baseline. The ensemble-mean end-of-century snowfall projection is less than 20% of baseline at low elevations, about 30% for moderate elevations, and less than

40% for high elevations. Thus, even at the highest elevations, the majority of snowfall is lost. In contrast to RCP8.5, the RCP2.6 scenario sees a negligible snowfall change at end-of-century compared with mid-century, also consistent with Fig. 8. The ensemble-mean results for the three sampled elevations are summarized in Table 4.

To provide a comprehensive view of the snowfall change and its dependence on elevation, and the uncertainties associated with our analysis, we show the remaining annual accumulated snowfall binned by elevation in Fig. 10, with a bin size of 250 feet. The mid-century and end-of-century projections for the two emissions scenarios are presented. The exact estimates of the uncertainty range are depicted as ± 1 standard deviation of the variability across all GCM projections, meaning there is a 68% probability the change in snowfall will lie in that range. In general, this figure tells a very similar story about snowpack loss and dependence on emissions scenario as Figs. 8 and 9. Fig. 10 does clarify that for all four cases, the percentage of snowfall loss decreases monotonically as elevation increases and roughly remains relatively constant above 7500 feet.

The uncertainty range, roughly 15–30 percentage points, generally decreases significantly as elevation increases (e.g., Figs. 10a, b, and d) because of the smaller sensitivity of snowfall to temperature variations when they occur further below the freezing point of water, as discussed above. There is one exception, where the uncertainty range is narrower at low elevations in the RCP8.5 end-of-century case. This arises from the fact that low-elevation areas receiving snow have essentially dwindled to zero at this time in the most sensitive models. In these instances, it does not matter how much warming occurs because the snow has disappeared.

The greater percentage snowfall loss at lower elevations in all future climate states probably accounts for the variation in snowfall loss across the region's mountain complexes (see Table 3). For example, for both time slices and both scenarios, the San Jacinto and San Bernardino mountains have somewhat less snowfall loss than the San Gabriel Mountains and especially the San Emigdio/Tehachapi complex. These higher elevation mountain ranges seem to be relatively insulated from snowpack loss throughout the 21st century. On the other hand, the comparatively low-lying San Emigdio/Techachapi complex appears to be somewhat more vulnerable to loss of snowfall.

7 Summary and Discussion

In this study, we used a combination of dynamical and statistical downscaling techniques to produce 2-km-resolution projections of future snowfall in the Los Angeles region in the middle and at the end of the 21st century. We generated these projections for two distinct greenhouse gas emissions scenarios: the RCP 8.5 scenario, representing "business as usual" emissions, and the RCP 2.6 scenario, representing a "mitigation" situation in which greenhouse gas emissions are aggressively reduced in the coming decades.

We first used the WRF regional climate model to simulate snowfall during a baseline period (1981–2000). We validated this baseline simulation against observational data from four representative points in the region. We then dynamically downscaled 5 GCMs to simulate snowfall in the Los Angeles region at the mid-century period (2041–2060) under the RCP8.5 scenario. We built a statistical model based on relationships between snowfall and temperature seen in the baseline simulation. To validate this statistical model, we compared its snowfall projections for mid-century under the RCP8.5 scenario with those of the 5 dynamically downscaled GCMs. We found that the statistical model's results closely tracked those of the 5 sample GCMs. We then used it to downscale: (1) the remaining GCMs to produce projections for the mid-century period, (2) all GCMs for an end-of-century (2081–2100) period under the RCP 8.5 scenario, and (3) all GCMs for mid-century and end-of-century periods under the RCP2.6 scenario.

Analyzing these data, we found that by mid-century, the mountainous areas in the Los Angeles region are likely to receive substantially less snowfall than in the baseline period. In RCP8.5, about 60% of the snowfall is likely to persist on average, while in RCP2.6, the amount remaining is somewhat higher (70%). After mid-century, however, the two scenarios diverge significantly. By end-of-century in the RCP8.5 scenario, snowfall sees a dramatic further reduction from mid-century levels, with only about a third of the baseline snowfall remaining. For RCP2.6, on the other hand, snowfall sees only a negligible further reduction from mid-century. Based on the spread in the statistically downscaled results, these figures are all associated with uncertainty, in the range of 15–30 percentage points. For both scenarios and both time slices, the snowfall loss is consistently greatest at low elevations, and the lower-lying mountain ranges are somewhat more vulnerable to snowfall loss.

The effect of snowfall loss on streamflow from mountain snow will be magnified by warming-accelerated melting of the already reduced snowpack. A comprehensive assessment of the snowmelt dimension of climate change in the Los Angeles region is beyond the scope of this

study. However, it is possible to make meaningful inferences based on simulated snow cover from the five dynamically downscaled GCMs of mid-century climate under RCP8.5. In these five simulations, seasonal snow cover disappears from the landscape on average 16 days earlier in the spring, almost exclusively due to enhanced snowmelt. (Individual results for the five simulations are as follows: CCSM4, 7 days earlier; CNRM-CM5, 10 days; MPI-ESM-LR, 16 days; GFDL-CM3, 21 days; MIROC-ESM-CHEM, 24 days.) If we had snow cover data for RCP2.6 mid-century, it probably would show a comparable acceleration of snowmelt. Thus the mid-century loss of snowpack would be significantly greater than the 30–40% likely loss due to snowfall reduction, especially in springtime.

Given that the warming and snowfall loss under RCP8.5 by end-of-century are roughly double the corresponding values for mid-century, the disappearance of snow cover from the landscape under RCP8.5 at end-of-century would probably be accelerated by about one month. This back-of-the-envelope calculation is comparable to observed shift in California snowmelt timing in response to warming (Kapnick and Hall 2010). Since RCP8.5 end-of-century snowfall is only a third of the baseline, and because this remaining snow would melt so much sooner, we conclude that under a business-as-usual emissions scenario, it is likely that toward century's end, snowpack would be found only at the very highest elevations during the coldest months.

Our downscaling and associated analysis reveal how the stark contrast between the global warming outcomes of the two emissions scenarios by century's end corresponds to a dramatic difference in snowfall and snowpack outcomes in the mountains of the Los Angeles region. From our projections, it is clear that roughly a third of snowfall, and a somewhat greater amount of snowpack, are likely to be lost by mid-century, no matter how aggressively greenhouse gas emissions are reduced. By end-of-century, however, the choice of emissions scenario does make a difference. Our results suggest that the likely 60–70% snowfall loss at the end-of-century, and the corresponding near-disappearance of the snowpack, can be substantially mitigated by aggressively reducing greenhouse gas emissions.

Figures

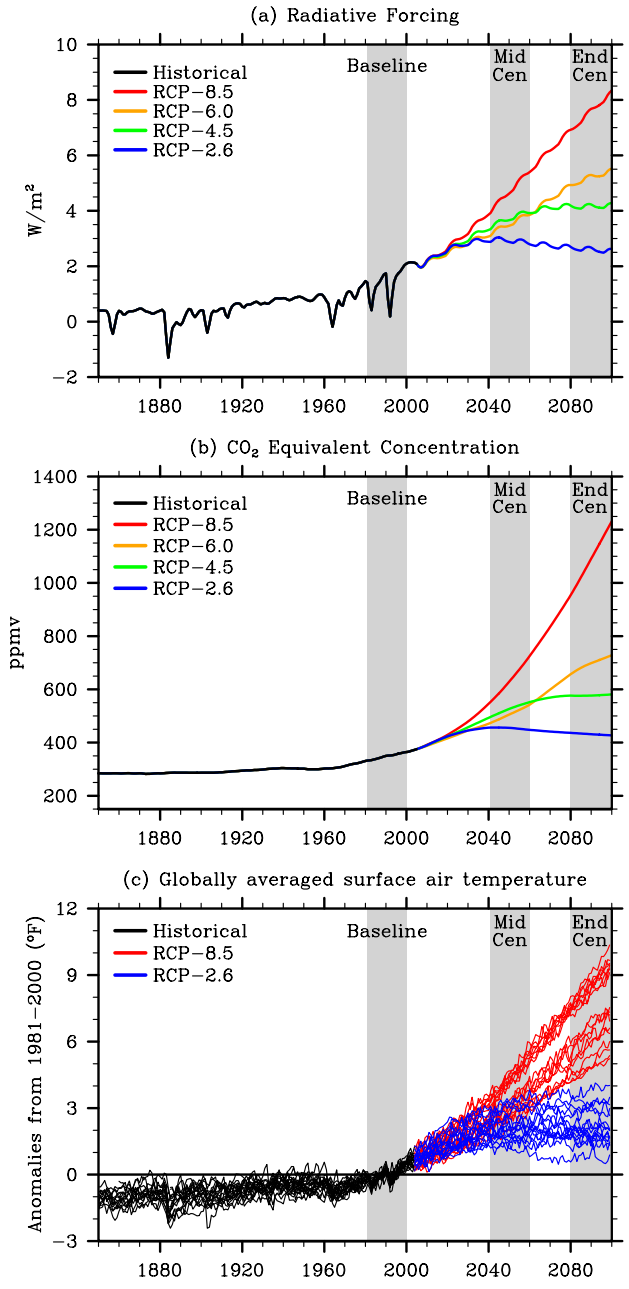

Fig. 1: (a) Total radiative forcing (anthropogenic plus natural) and (b) Carbon dioxide (CO_2) equivalent concentrations for approximately the past century and four Representative Concentration Pathways: RCP8.5, RCP6, RCP4.5 and RCP2.6 (also called RCP3-PD); (c) Global-mean surface air temperature departures from 1981–2000 mean as simulated in all CMIP5 GCMs used in this study for the historical forcing (black), and RCP8.5 (red) and RCP2.6 (blue). Gray shaded regions denote the baseline (1981–2000), mid-century (2041–2060), and end-of-century (2081–2100) periods used in this study.

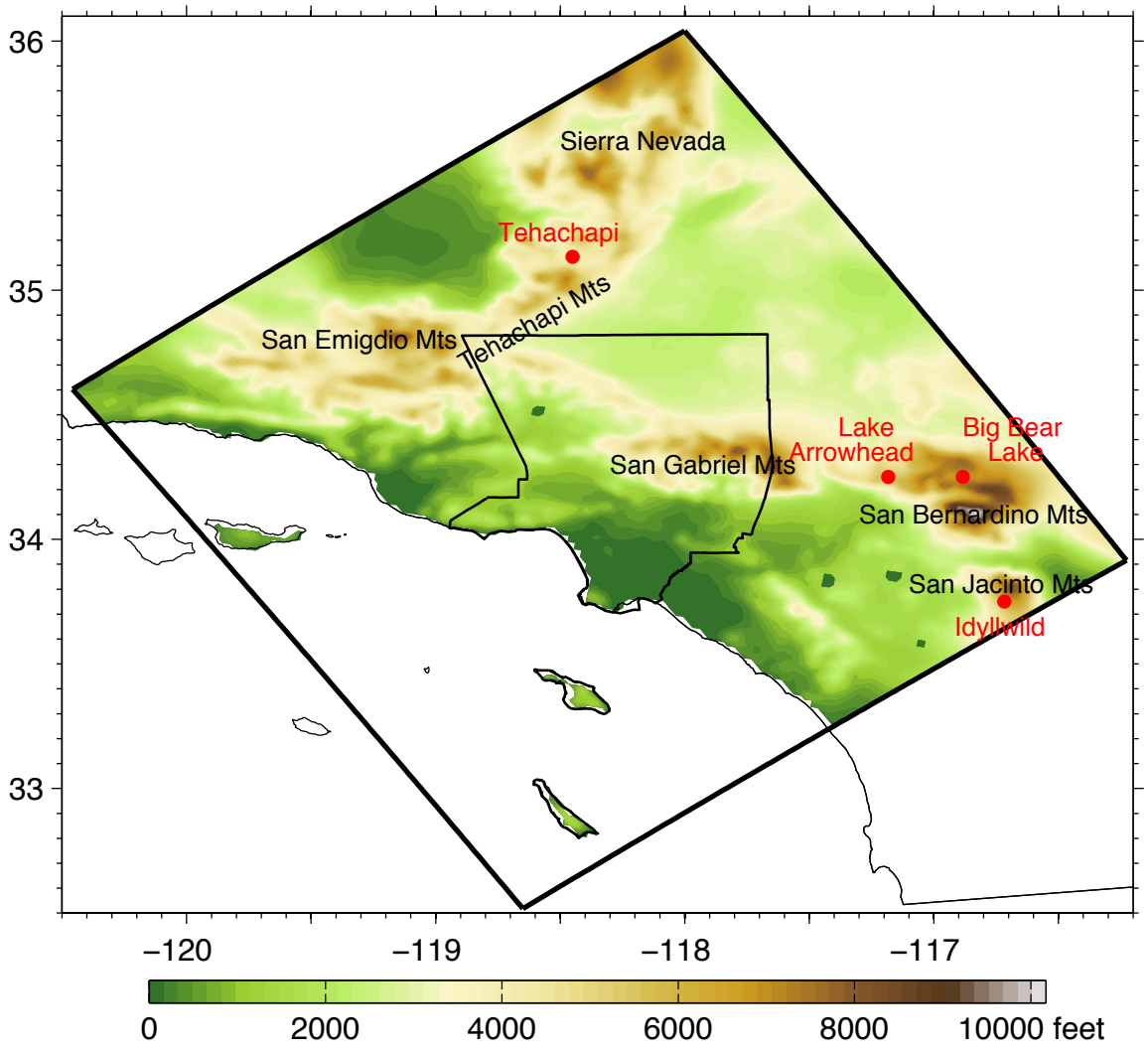

Fig. 2: Topography of the innermost domain, shown in color at the domain's 2-km resolution. The border of Los Angeles County is also shown. Red dots represent point measurement sites, whose observations are used to validate the dynamically downscaled baseline climate simulation. Prominent mountain ranges within the model domain are also shown.

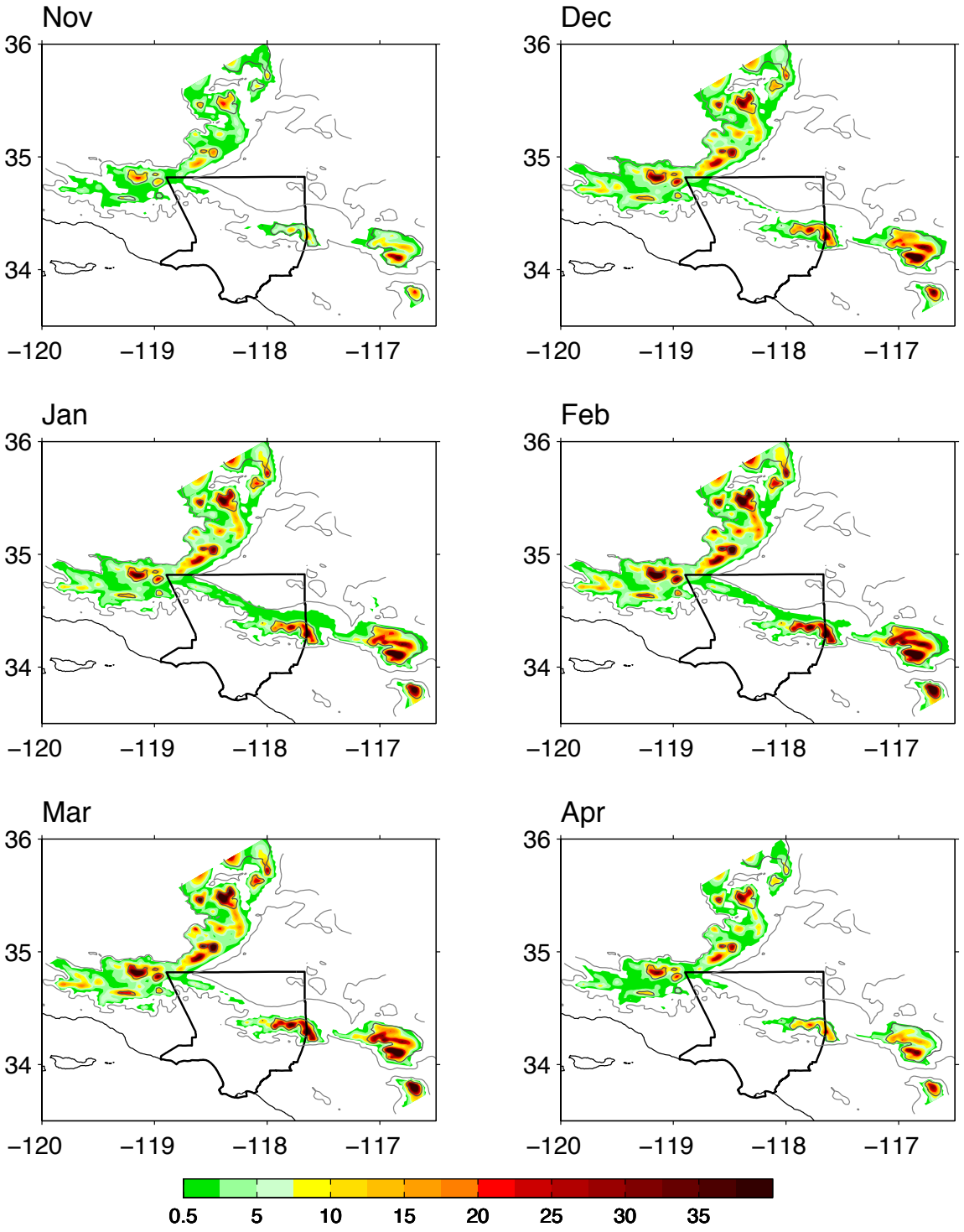

Fig. 3: Simulated baseline (1981–2000) monthly snowfall (unit: inches/month) climatology for wet months. Topography contour lines at 3000 and 6000 feet are highlighted. Note that the model provides snowfall in terms of liquid water equivalent. To generate these snowfall values in terms of snow depth, we used a constant snow density value provided by Baxter et al. (2005). See Section 4.2 for details.

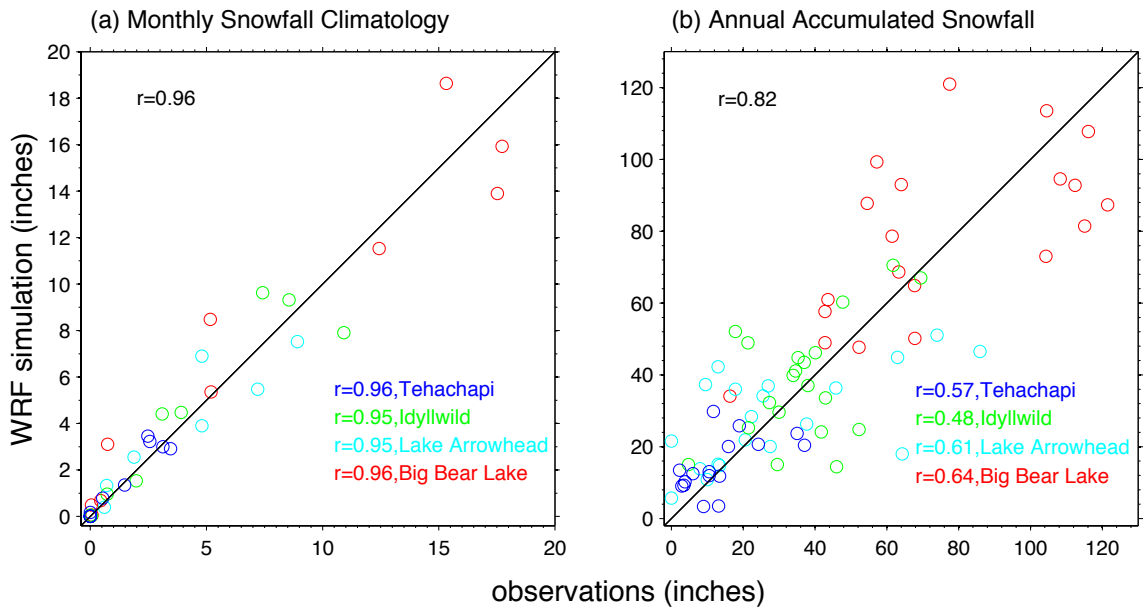

Fig. 4: Scatter plots between observed snowfall and simulated snowfall (converted from snow liquid water equivalent to inches) at four sites: Tehachapi, Idyllwild, Lake Arrowhead, and Big Bear Lake. Left panel: baseline period (1981–2000) monthly snowfall climatology; Right panel: annual accumulated snowfall.

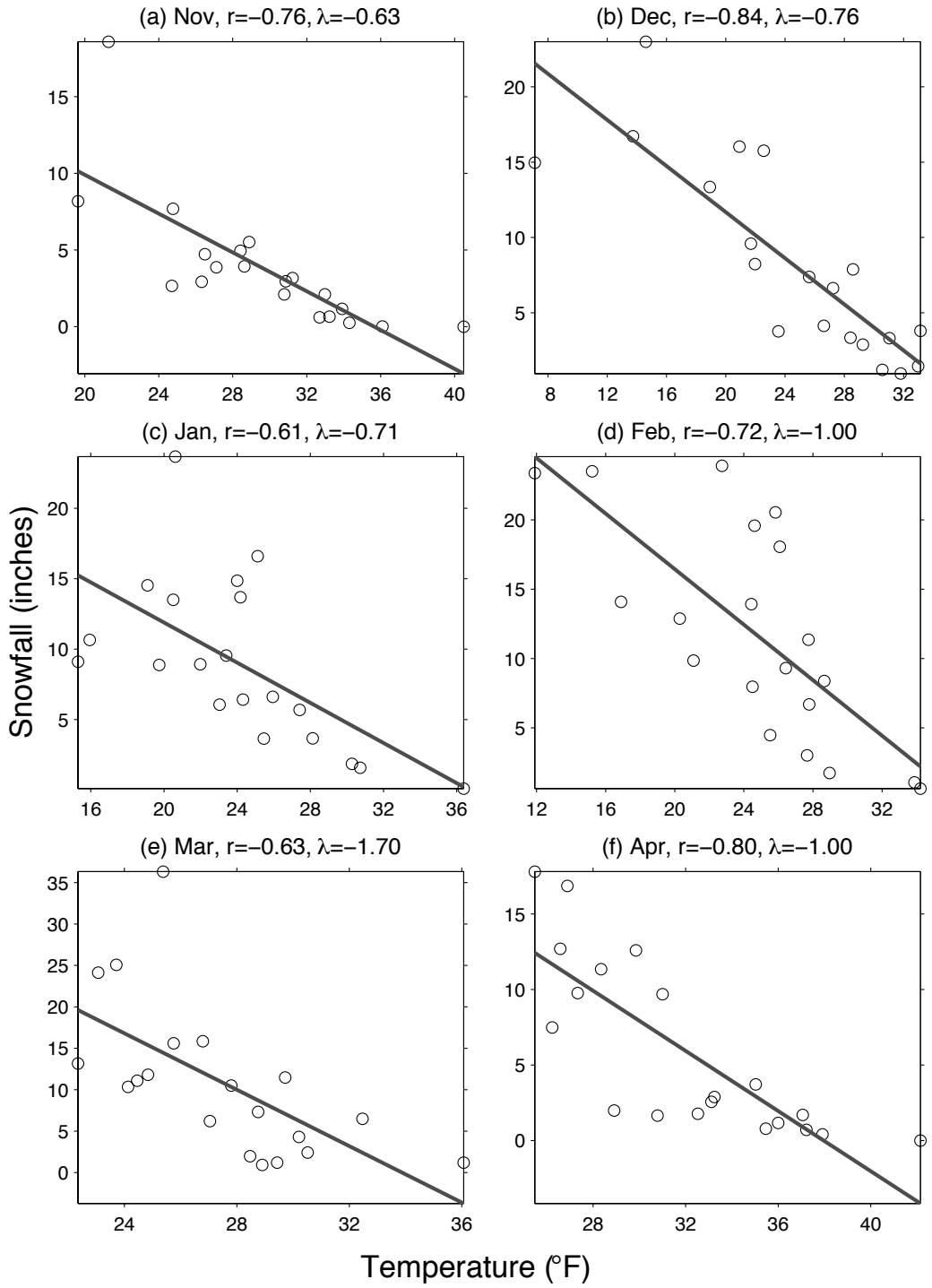

Fig. 5: Scatter plots between monthly accumulated snowfall (unit: inches) at locations between 5750 and 6000 feet and the average surface air temperature of the coldest day of the month. Only the six wet months of the year are shown. Each circle represents one year of the baseline period (1981–2000). This figure illustrates how the snowfall statistical model can be developed based on minimum temperature inputs. The Greek letter λ denotes the slope of the regression line dS / dT_{min}.

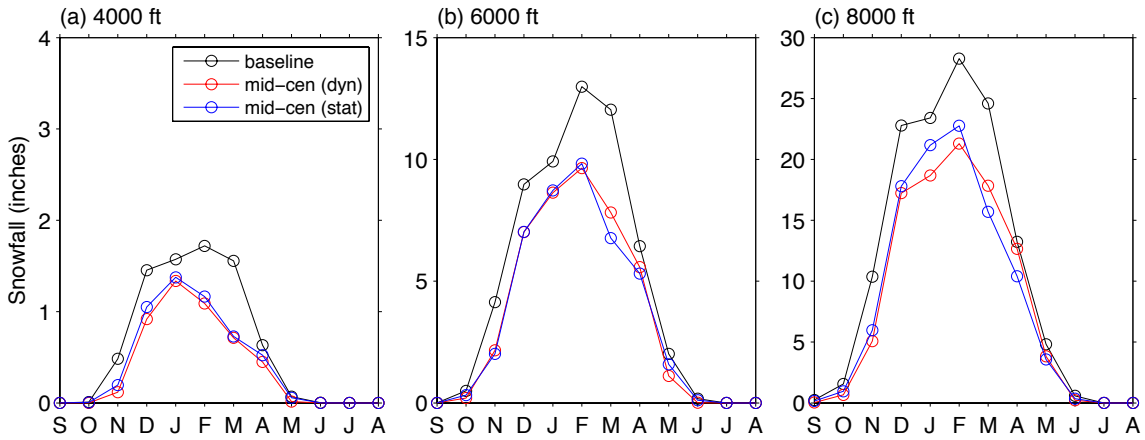

Fig. 6: Seasonal cycles of snowfall (unit: inches) for three elevations (unit: feet). Shown are data from the dynamically downscaled results for the baseline (1981–2000) period (black); the mid-century (2041–2060) dynamically downscaled projections of CCSM4 under RCP 8.5 (red); and the corresponding mid-century statistically downscaled projections (blue).

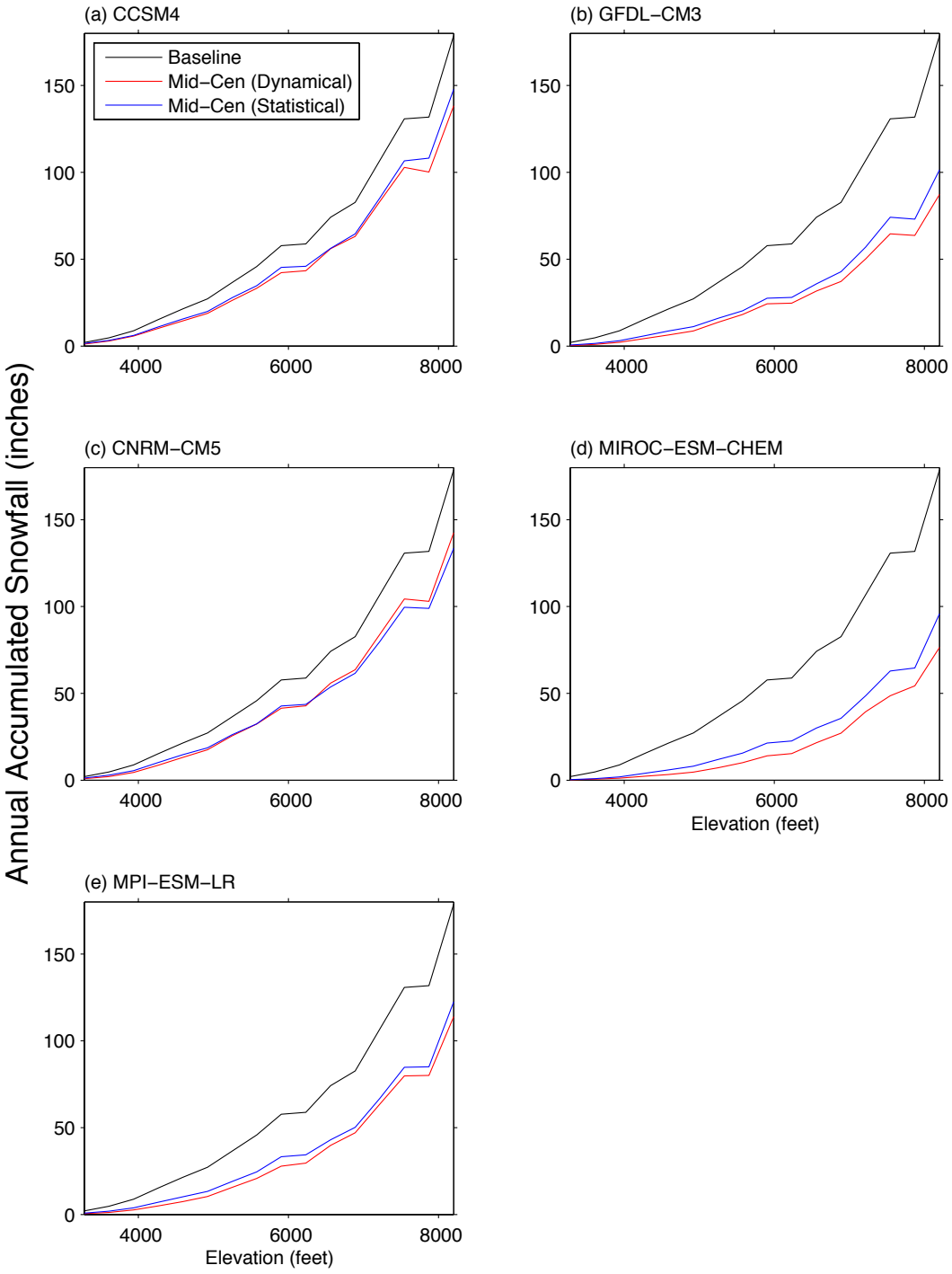

Fig. 7: Annual accumulated snowfall (unit: inches) for five WRF-GCM simulations binned by elevation (unit: feet). Shown are the dynamically downscaled baseline simulation (black); the dynamically downscaled mid-century projections under RCP 8.5 (red); and the corresponding statistically downscaled mid-century projections (blue).

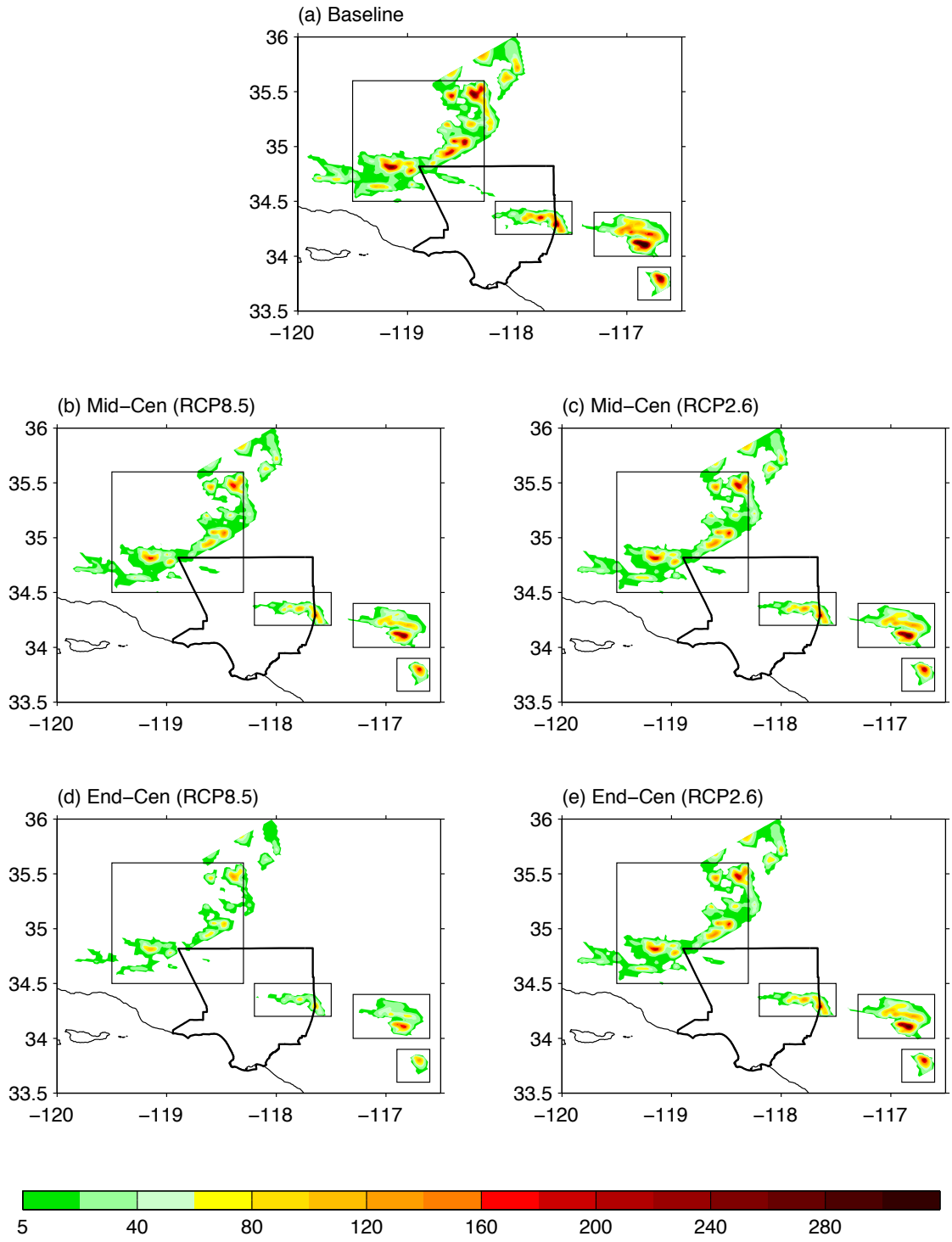

Fig. 8: Annual accumulated snowfall (unit: inches) for (a) the baseline simulation and projections for (b) mid-century period (2041–2060) under RCP8.5; (c) mid-century period under RCP2.6; (d) end-of-century period (2081–2100) under RCP8.5; and (e) end-of-century period under RCP2.6. Only areas with annual accumulated snowfall of more than 5 inches are colored. The borders of Los Angeles County are shown, and boxes highlight individual mountain areas. From left to right, these areas are the San Emigdio/Tehachapi Mountains, the San Gabriel Mountains, the San Bernardino Mountains (upper right), and the San Jacinto Mountains (lower right). For larger images of each area, see Appendix II.

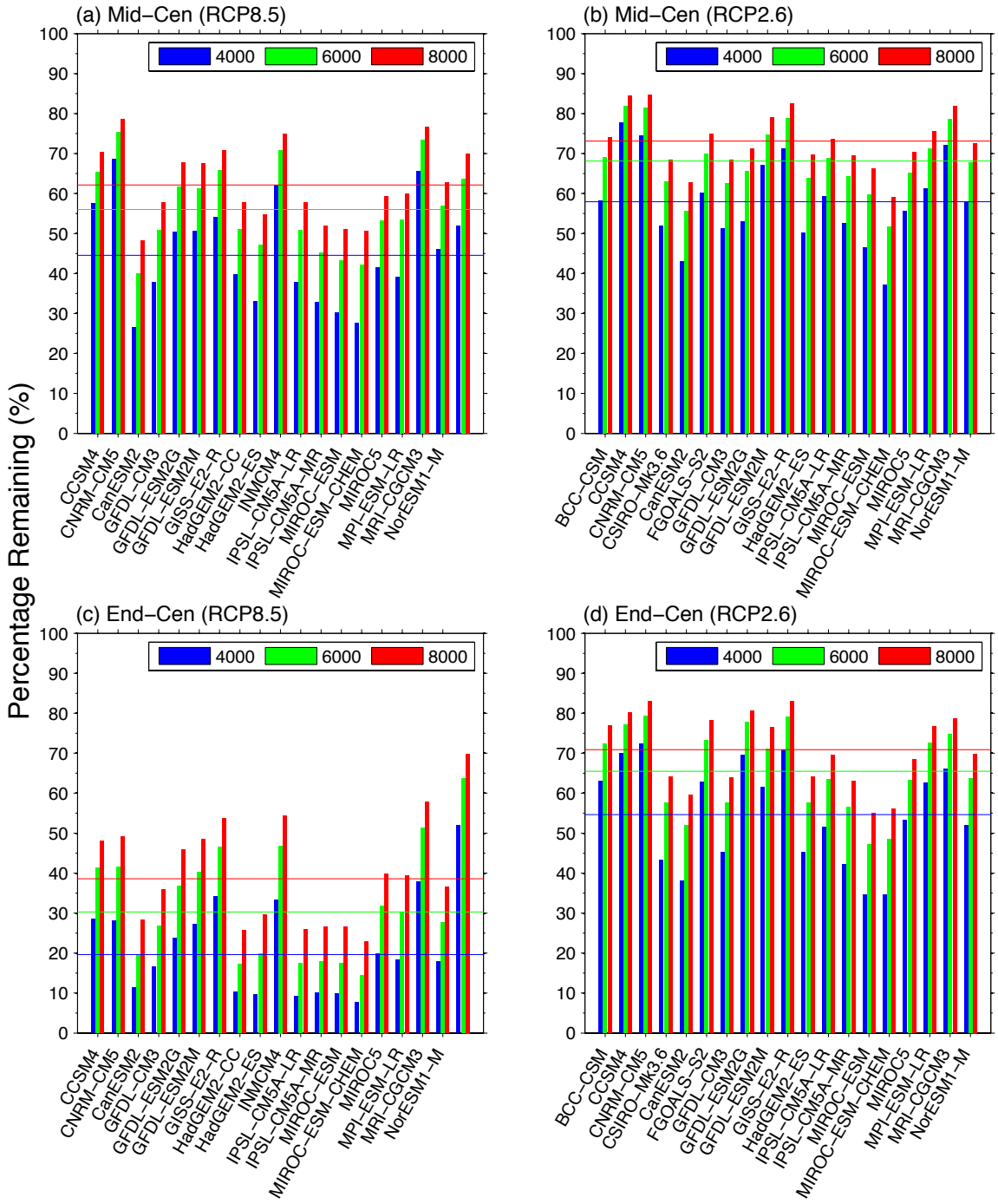

Fig. 9: Remaining annual accumulated snowfall (expressed as percentage of future snowfall to baseline snowfall) for each GCM at three elevations (4000, 6000, and 8000 feet, representing low, moderate, and high elevations). Horizontal lines denote the corresponding ensemble-mean across all GCMs. Upper left panel: mid-century period (2041–2060) under RCP8.5; Upper right panel: mid-century period under RCP2.6; Bottom left panel: end-of-century period (2081–2100) under RCP8.5; Bottom right panel: end-of-century period under RCP2.6.

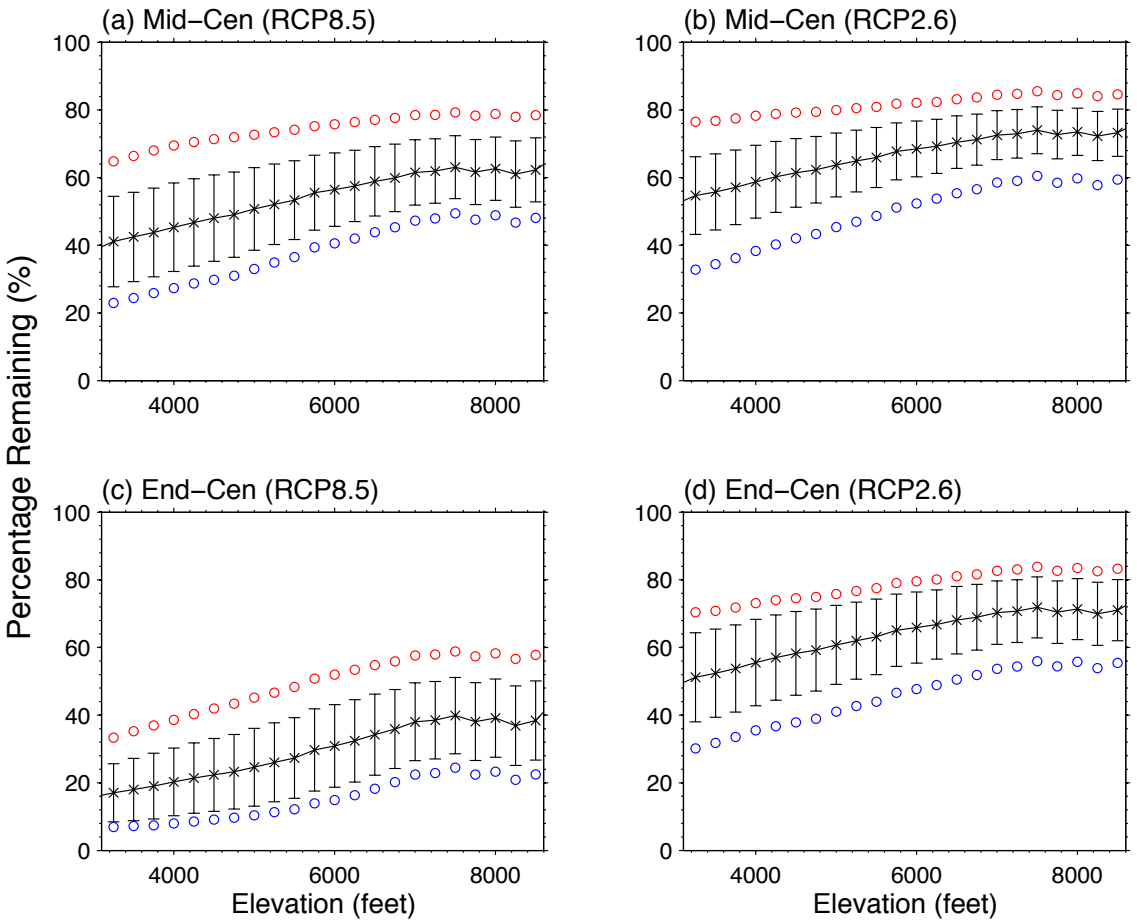

Fig. 10: Remaining annual accumulated snowfall (expressed as a percentage of future snowfall to baseline snowfall) binned by elevation. Shown are ensemble-mean values (cross) with ± 1 standard deviation of the variability across all GCMs (bar), along with maximum (red circle) and minimum (blue circle) values. Upper left panel: mid-century period (2040–2060) under RCP8.5; Upper right panel: mid-century period under RCP2.6; Bottom left panel: end-of-century period (2081–2100) under RCP8.5; Bottom right panel: end-of-century period under RCP2.6. Considering the small number of model grid cells above very high elevations (e.g., 8500 feet), we assume that sample size is too small to give statistically significant results. Thus, we present only results below 8500 feet.

Tables

Table 1: Name and identifying information (country, institution, and resolution) of the CMIP5 GCMs used for climate downscaling. All GCMs are statistically downscaled, whereas only CCSM4, GFDL-CM3, CNRM-CM5, MIROC-ESM-CHEM, and MPI-ESM-LR are dynamically downscaled. The availability of the RCP2.6 and RCP8.5 emissions scenarios is also indicated. Note: 1° is approximately 100 km.

MODEL	COUNTRY	INSTITUTE	RESOLUTION	RCP2.6	RCP8.5
BCC-CSM	China	Beijing Climate Center, China Meteorological Administration	2.8° x 2.8°	✓	
CCSM4	USA	National Center for Atmospheric Research	1.25° x .9°	✓	✓
Can-ESM2	Canada	Canadian Centre for Climate Modelling and Analysis	2.8° x 2.8°	✓	✓
CNRM-CM5	France	Centre National de Recherches Meteorologiques	1.4° x 1.4°	✓	✓
CSIRO-Mk3.6	Australia	Commonwealth Scientific and Industrial Research Organization	1.9° x 1.9°	✓	
FGOALS-S2	China	LASG, Institute of Atmospheric Physics, Chinese Academy of Sciences	2.8° x 1.7°	✓	
GFDL-CM3	USA	NOAA Geophysical Fluid Dynamics Laboratory	2.5° x 2.0°	✓	✓
GFDL-ESM2M	USA	NOAA Geophysical Fluid Dynamics Laboratory	2.5° x 2.0°	✓	✓
GFDL ESM2G	USA	NOAA Geophysical Fluid Dynamics Laboratory	2.5° x 2.0°	✓	✓
GISS-E2-R	USA	NASA Goddard Institute for Space Studies	2.5° x 2.0°	✓	✓
HadGEM2-CC	UK	Met Office Hadley Centre	1.9° x 1.25°		✓
HadGEM2-ES	UK	Met Office Hadley Centre	1.9° x 1.25°	✓	✓
INMCM4	Russia	Institute for Numerical Mathematics	2.0° x 1.5°		✓
IPSL-CM5A-LR	France	Institut Pierre Simon Laplace	3.75° x 1.9°	✓	✓
IPSL-CM5A-MR	France	Institut Pierre Simon Laplace	2.5° x 1.25°	✓	✓
MIROC-5	Japan	AORI (U. Tokyo), NIES, JAMESTEC	1.4° x 1.4°	✓	✓
MIROC-ESM-CHEM	Japan	AORI (U. Tokyo), NIES, JAMESTEC	2.8° x 2.8°	✓	✓
MIROC-ESM	Japan	AORI (U. Tokyo), NIES, JAMESTEC	2.8° x 2.8°	✓	✓
MPI-ESM-LR	Germany	Max Planck Institute for Meteorology	1.9° x 1.9°	✓	✓
MRI-CGCM3	Japan	Meteorological Research Institute	1.1° x 1.1°	✓	✓
NorESM1-M	Norway	Norwegian Climate Center	2.5° x 1.9°	✓	✓

Table 2: Summary of information associated with observational stations from National Weather Service (NWS) Cooperative Observer Program (COOP) used to validate the baseline simulation.

Station Name	NWS COOP ID	Latitude	Longitude	Elevation (feet)	Elevation in WRF (feet)	Observational Period
Big Bear Lake	040741	34’15’’	116’53’’	6790	6842	1960/07-2005/12
Lake Arrowhead	044671	34’15’’	117’11’’	5200	5312	1941/08-2011/11
Idyllwild	044211	33’45’’	116’43’’	5380	5346	1943/10-2012/09
Tehachapi	048826	35’08’’	118’27’’	4020	4025	1893/01-1997/06

Table 3: Baseline snowfall and most likely (ensemble-mean across GCMs) future snowfall averaged over domain and its percentage (in parentheses) to the baseline. Unit: inches/year.

	Entire domain	San Emigdio/ Tehachapi	San Gabriel	San Bernardino	San Jacinto
Baseline	42.8	39.9	49.7	65.4	68.4
RCP8.5 Mid-century	24.7 (58%)	22.3 (56%)	29.4 (59%)	40.5 (62%)	41.2 (61%)
RCP8.5 End-of-century	14.3 (33%)	12.5 (31%)	17.2 (35%)	25.3 (39%)	25.8 (38%)
RCP2.6 Mid-century	29.7 (69%)	27.1 (68%)	35.1 (71%)	47.7 (73%)	49.3 (72%)
RCP2.6 End-of-century	28.6 (67%)	26.1 (65%)	33.9 (68%)	46.3 (71%)	47.8 (70%)

Table 4: Most likely (ensemble-mean across GCMs) ratio of future snowfall to baseline snowfall. Baseline: 1981–2000; Mid-Century: 2041–2060; End-of-Century: 2081–2100.

	RCP8.5 (Mid-Cen)	RCP8.5 (End-Cen)	RCP2.6 (Mid-Cen)	RCP2.6 (End-Cen)
4000 feet (low)	45%	20%	58%	55%
6000 feet (mid)	56%	30%	68%	66%
8000 feet (high)	62%	39%	73%	71%

Appendix I: Inclusion of Precipitation as a Predictor in the Statistical Model

In the main part of this study, we presented a statistical model of snowfall based on the sensitivity of snowfall to minimum temperature. We then used the future regional temperature changes associated with the two scenarios and time slices to project future snowfall changes. However, precipitation may also change in the future, and future snowfall may also be affected by this change. For example, Fig. A1 shows the annual accumulated precipitation changes in the five dynamically-downscaled simulations. Clearly there is a variety of responses, and in some cases the changes are not small in magnitude.

To test whether these precipitation changes are competitive with warming in their impact on snowfall, we built another statistical model that includes precipitation as a predictor. This model is identical to our temperature-only model, except there is another term corresponding to the sensitivity of snowfall to precipitation:

$$S = \frac{dS}{dT_{min}} T_{min} + \frac{dS}{dP} P + B$$

Here P is monthly-mean precipitation, and dS/dP is the sensitivity of monthly-mean snowfall to monthly-mean precipitation. Similar to the temperature-only model, we perform multiple linear regression on data from the baseline simulation to calculate dS/dT_{min} and dS/dP.

In exact analogy with the temperature-only statistical model, we then generate future snowfall projections using future changes in temperature and precipitation as predictors:

$$\Delta S = \frac{dS}{dT_{min}} \Delta T_{min} + \frac{dS}{dP} \Delta P$$

Next we compare statistical predictions of future snowfall change given by the temperature-only model presented in the main text and the temperature/precipitation model described in this Appendix against those of the dynamical downscaling experiments. In analogy to the main text, we first present the performance of the statistical models in recovering the future change in the full seasonal cycle of snowfall for a single downscaled GCM: CCSM4. Then we present results for the other dynamically downscaled GCMs, but to be concise, we do so for annual accumulated snowfall only.

Fig. A2 is a companion figure to Fig 6, and shows the two statistically downscaled mid-21st century seasonal cycles of snowfall under the RCP8.5 scenario and the corresponding dynamically downscaled results for CCSM4. It is clear that seasonal cycle of the temperature/precipitation statistical model tracks that of the temperature-only regression model

fairly closely, within a few percent in most cases. The snowfall reduction from baseline is also well-captured by the temperature-only model. This is a strong confirmation that the temperature is the dominant predictor for snowfall in the CCSM4 downscaling. Fig. A3 is a companion figure to Fig. 7, and shows a comparison of statistically and dynamically downscaled results for annual accumulation, now for all five dynamically downscaled models. As in Fig. A2, the temperature/precipitation statistical model generally tracks the temperature-only model to within a few percent. The annual snowfall loss implied by the two statistical models is also nearly identical.

These results are strong confirmation that minimum temperature is the dominant predictor for snowfall in all dynamical downscaling experiments. This analysis provides additional confidence that the temperature-only statistical model used in the main text provides snowfall projections that are very close to those that would result if dynamical downscaling were undertaken.

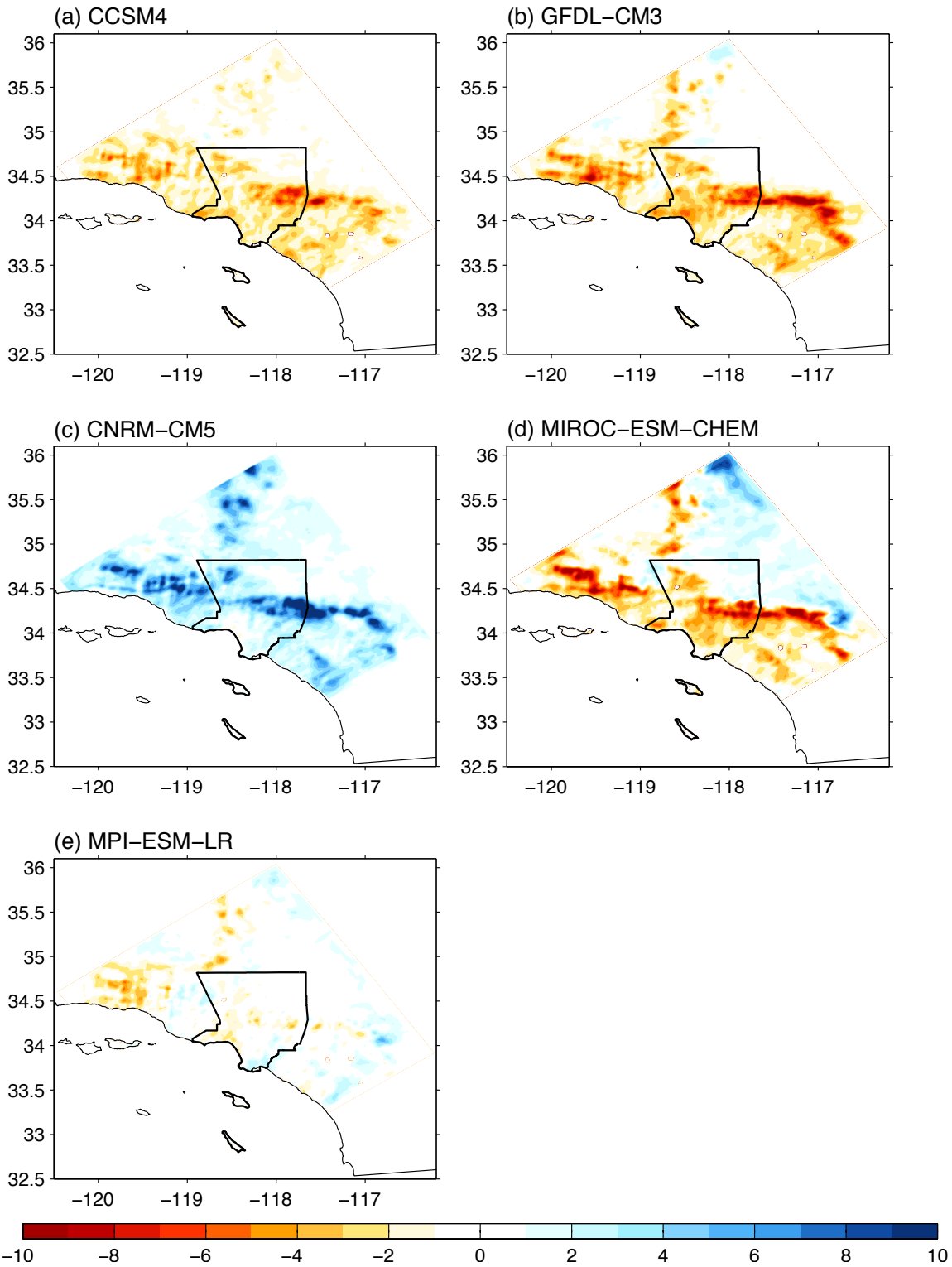

Fig. A1: Annual accumulated precipitation changes (unit: inches) at mid-century under RCP 8.5 in the dynamically downscaled simulations for (a) CCSM4, (b) GFDL-CM3, (c) CNRM-CM5, (d) MIROC-ESM-CHEM and (e) MPI-ESM-LR.

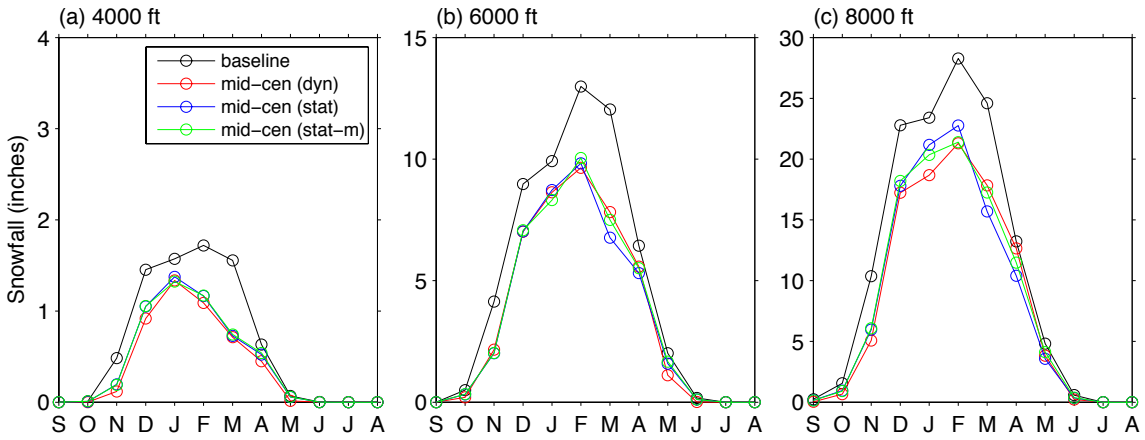

Fig. A2: Seasonal cycles of snowfall (unit: inches) for three elevations (unit: feet). Shown are data for the dynamically downscaled results for the baseline (1981–2000) period (black); the mid-century (2041–2060) dynamically downscaled projection of CCSM4 under RCP 8.5 (red); the corresponding mid-century statistically downscaled projection using temperature as the sole predictor (blue); and the corresponding mid-century statistically downscaled projection using both temperature and precipitation as predictors (green).

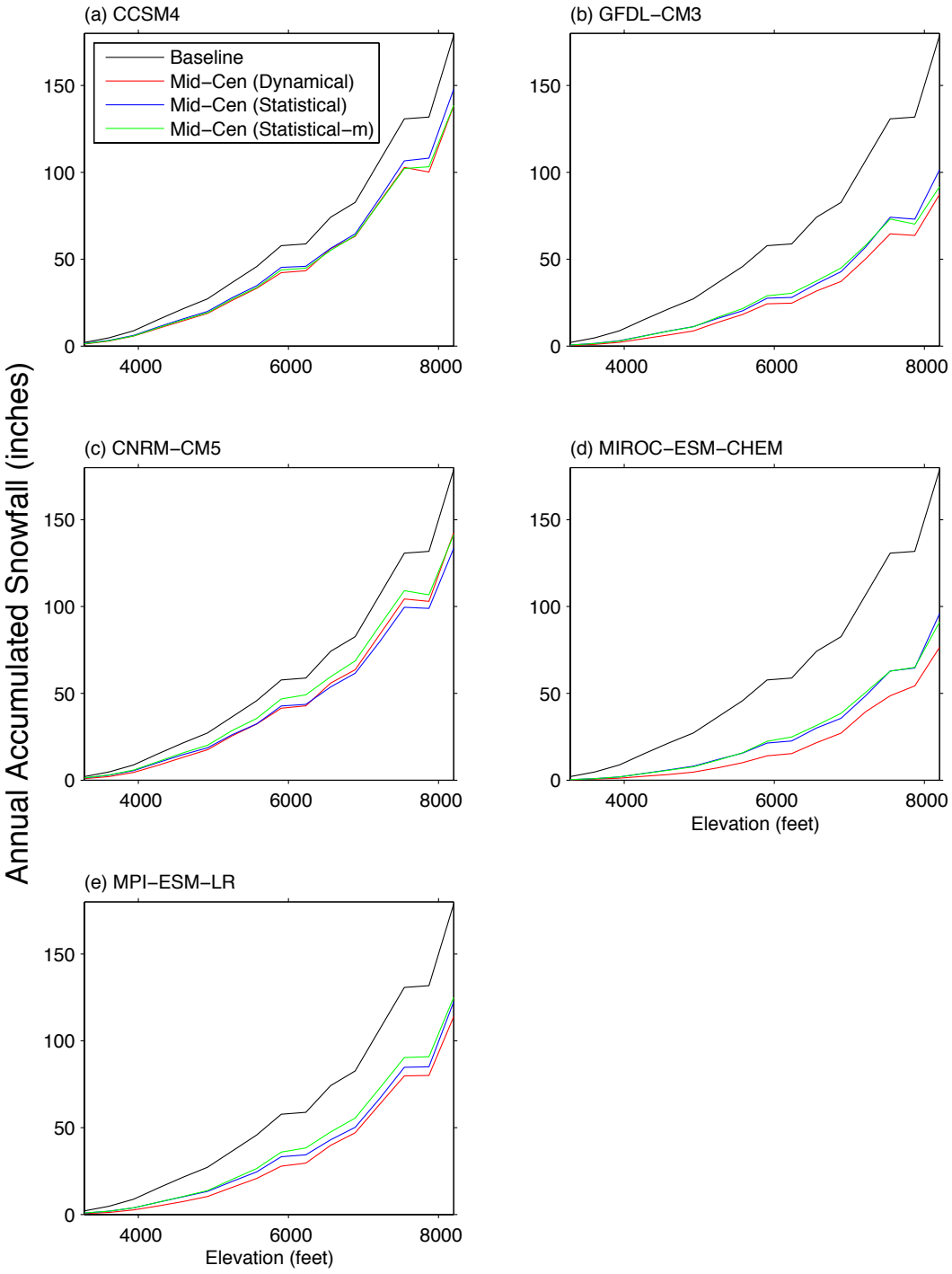

Fig. A3: Annual accumulated snowfall (unit: inches) for five WRF-GCM simulations binned by elevation (unit: feet). Shown are the dynamically downscaled baseline simulation (black); the dynamically downscaled mid-century projections under RCP8.5 (red); the corresponding statistically downscaled mid-century projection using temperature as the sole predictor (blue); and the corresponding statistically downscaled mid-century projection using both temperature and precipitation as predictors (green).

Appendix II: Spatial Patterns of Snowfall Changes in Mountain Areas

Here we provide, for the different mountain areas of the Los Angeles region, enlarged images of the spatial distribution of annual accumulated snowfall simulated for our baseline (1981–2000) period and projected for the mid-century (2041–2060) and end-of-century (2081–2100) periods under the two greenhouse gas emissions scenarios. For the future time slices, snowfall values depicted are the ensemble-mean, i.e., an average over all the GCMs downscaled in this study representing the most likely projected annual accumulated snowfall. Note that the data presented here are identical to the data depicted in Fig. 8.

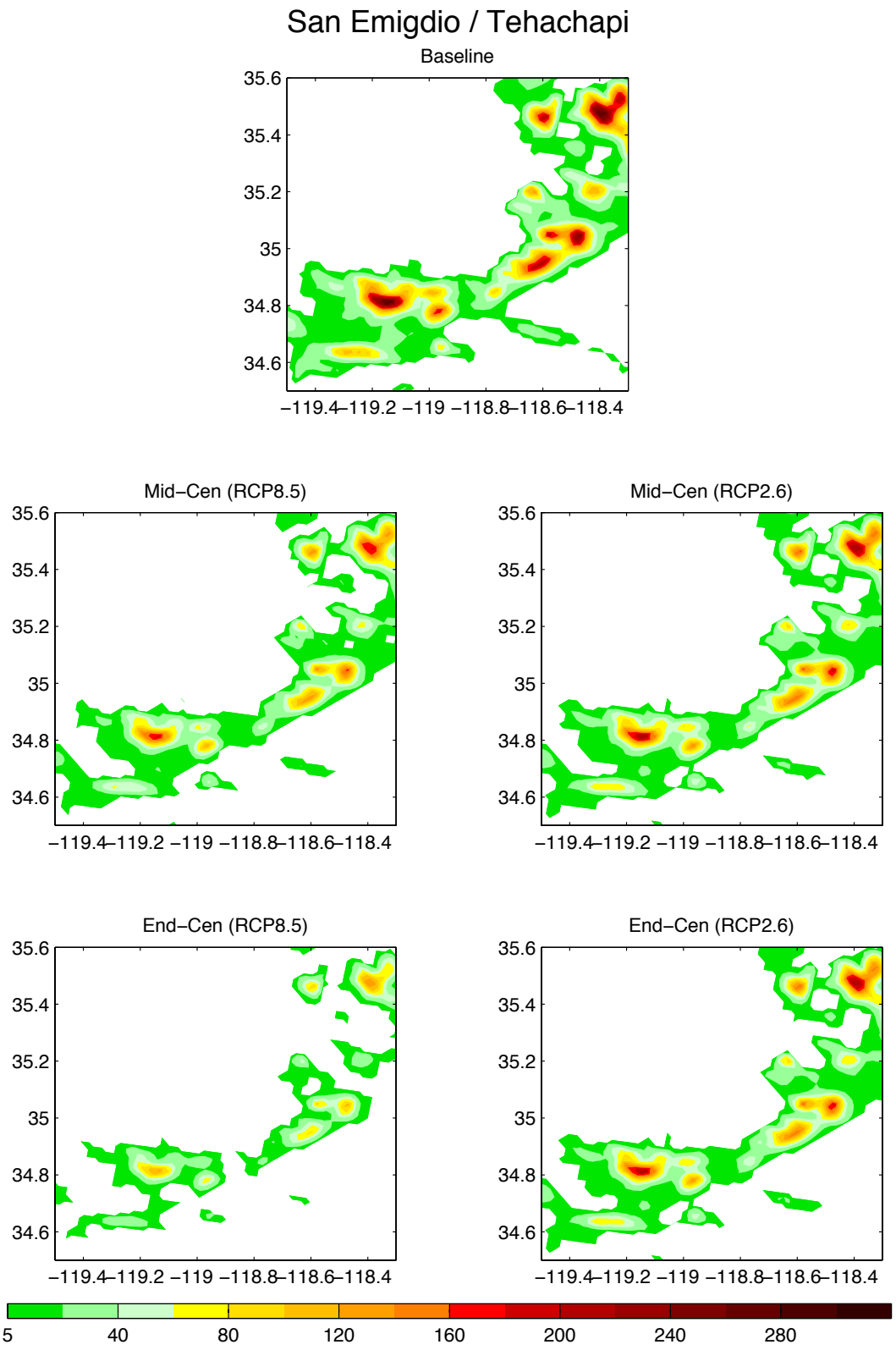

Fig. A4: Annual accumulated snowfall (unit: inches) in the San Emigdio and Tehachapi Mountains for (a) the baseline (1981–2000) simulation and projections for (b) mid-century period (2041–2060) under RCP8.5; (c) mid-century period under RCP2.6; (d) end-of-century period (2081–2100) under RCP8.5; and (e) end-of-century period under RCP2.6.

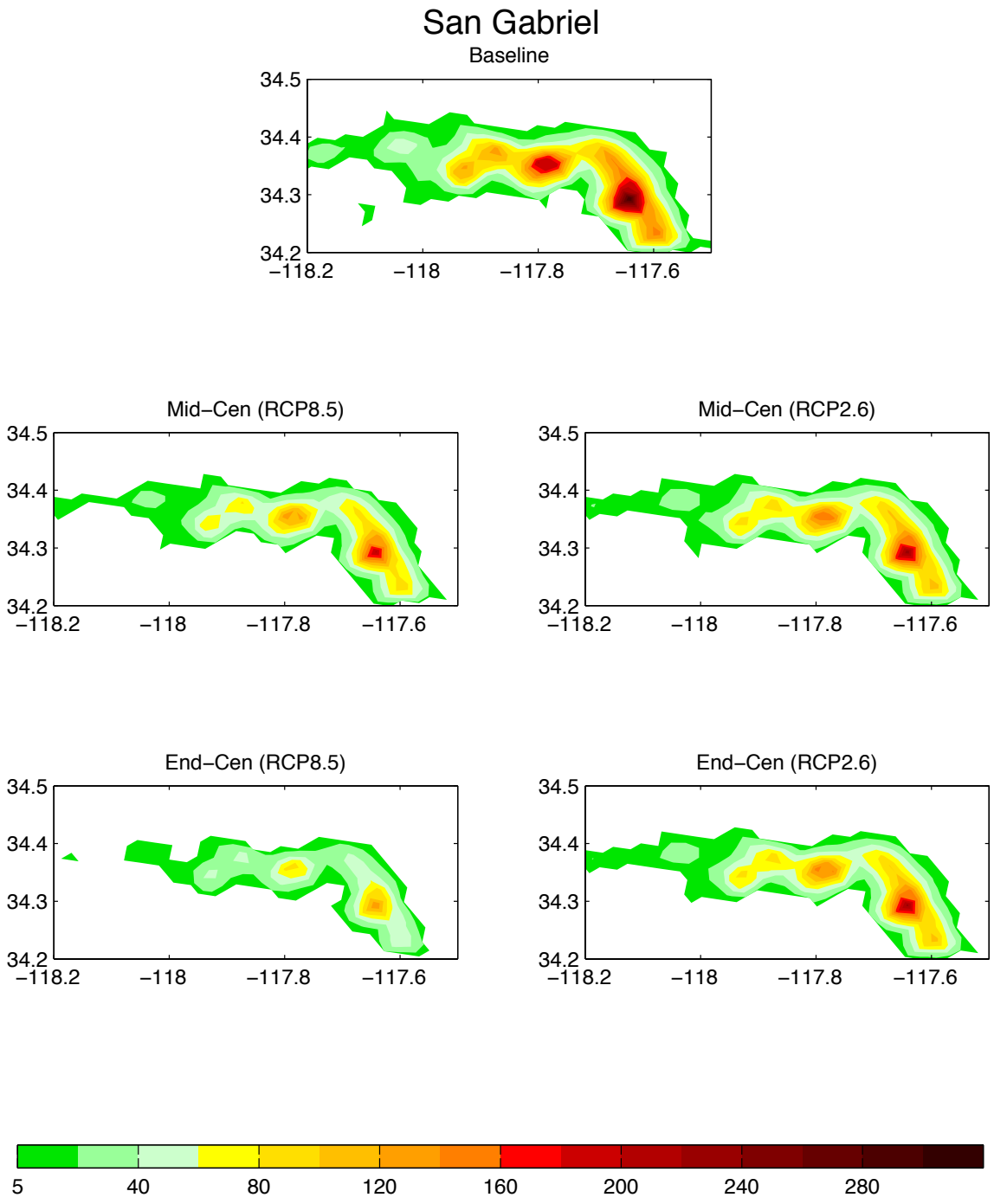

Fig. A5: Annual accumulated snowfall (unit: inches) in the San Gabriel Mountains for (a) the baseline (1981–2000) simulation and projections for (b) mid-century period (2041–2060) under RCP8.5; (c) mid-century period under RCP2.6; (d) end-of-century period (2081–2100) under RCP8.5; and (e) end-of-century period under RCP2.6.

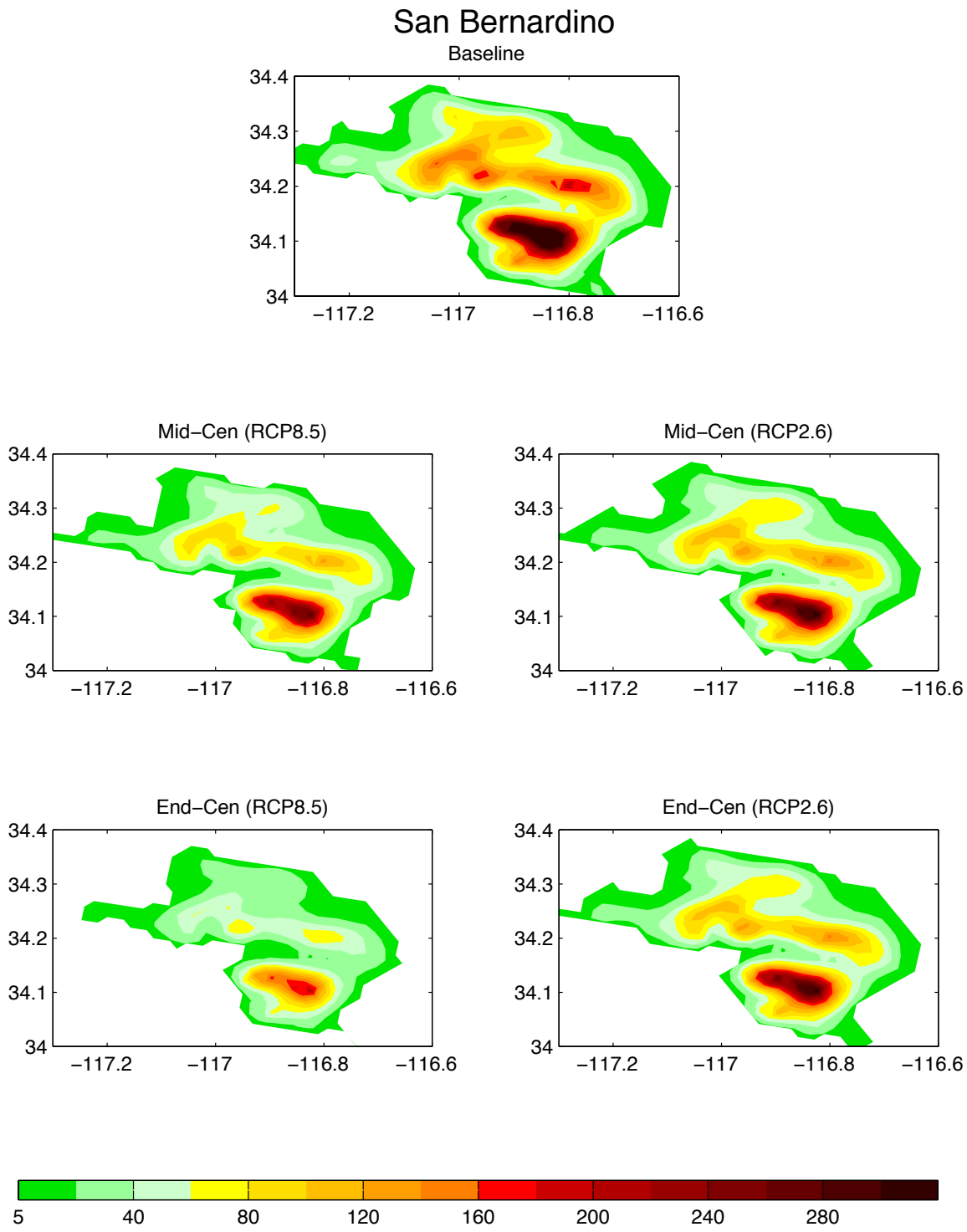

Fig. A6: Annual accumulated snowfall (unit: inches) in the San Bernardino Mountains for (a) the baseline (1981–2000) simulation and projections for (b) mid-century period (2041–2060) under RCP8.5; (c) mid-century period under RCP2.6; (d) end-of-century period (2081–2100) under RCP8.5; and (e) end-of-century period under RCP2.6.

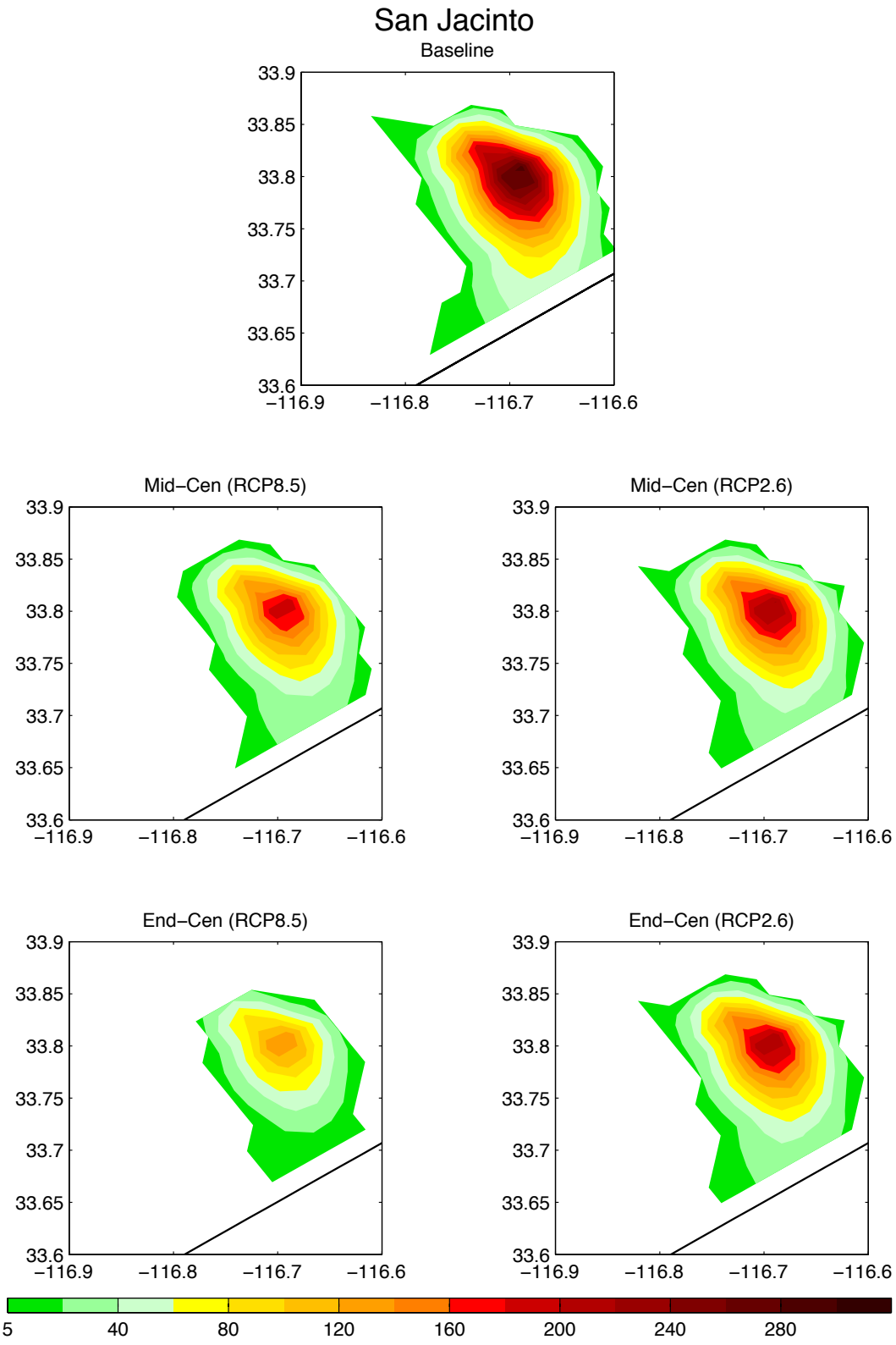

Fig. A7: Annual accumulated snowfall (unit: inches) in the San Jacinto Mountains for (a) the baseline (1981–2000) simulation and projections for (b) mid-century period (2041–2060) under RCP8.5; (c) mid-century period under RCP2.6; (d) end-of-century period (2081–2100) under RCP8.5; and (e) end-of-century period under RCP2.6. The straight line at the lower right corner of each panel marks the boundary of our 2-km model domain.

References

Bales, R. C., N. P. Molotch, T. H. Painter, M. D. Dettinger, R. Rice, and J. Dozier, 2006: Mountain hydrology of the western United States. Water Resour. Res., 42, W08432, doi:10.1029/2005WR004387.

Barnett, T. P., and Coauthors, 2008: Human-induced changes in the hydrology of the western United States. Science, 319, 1080–1083, doi:10.1126/science.1152538.

Baxter, M. A., C. E. Graves, and J. T. Moore, 2005: A climatology of snow-to-liquid ratio for the contiguous United States. Wea. Forecasting, 20, 729–744.

Brovkin, V., L. Boysen, T. Raddatz, V. Gayler, A. Loew and M. Claussen, 2012: Evaluation of vegetation cover and land-surface albedo in MPI-ESM CMIP5 simulations. Journal of Advances in Modelling Earth Systems, 4, doi:10.1029/2012MS000169, accepted.

Caldwell P., H.N.S. Chin, D.C. Bader, and G. Bala, 2009: Evaluation of a WRF dynamical downscaling simulation over California. Climatic Change, 95, 499–521.

Cayan D.R., 1996: Interannual climate variability and snowpack in the western United States, J. Climate, 9, 928-948.

Cayan, D.R, S. Kammerdiener, M.D. Dettinger, J.M. Caprio, and D.H. Peterson. 2001: Changes in the onset of spring in the western United States. Bulletin of the American Meteorological Society 82: 399–415.

Cayan, D.R., E.P. Maurer, M.D. Dettinger, M. Tyree and K. Hayhoe, 2008: Climate change scenarios for the California region. Climatic Change, 87, 21–42.

Chin H.S., 2008: Dynamical downscaling of GCM simulations: toward the improvement of fore-cast bias over California. LLNL-TR-407576, Lawrence Livermore National Lab. https://e-reports-int.llnl.gov/pdf/365755.pdf, 16pp.

Conil S., and A. Hall, 2006: Local regimes of atmospheric variability: A case study of Southern California. J. Climate, 19,4308-4325.

Donner, L. J. and coauthors, 2012: The dynamical core, physical parameterizations, and basic characteristics of the atmospheric component AM3 of the GFDL global coupled model CM3. Journal of Climate, 24, 3484–3519.

Gent, P. R., and coauthors, 2011: The Community Climate System Model version 4. J. Climate, 24, 4973–4991.

Giorgi, F., B. Hewitson, J. Christensen, M. Hulme, H. von Storch, P.Whetton, R. Jones, L. Mearns and C. Fu, 2001: Regional climate information-evaluation and projections. In: J.T. Houghton, Y. Ding, D.J. Griggs, M. Noguer, P.J. van der Linden, X. Dai, K. Maskell and C.A. Johnson (eds.). pp. 583–638. Climate Change 2001: The Scientific Basis. Contribution of Working Group I to the Third Assessment Report of the Intergovernmental Panel on Climate Change. Cambridge University Press.

Hall A, F Sun, D Walton, S Capps, X Qu, H-Y Huang, N Berg, A Jousse, M Schwartz, M Nakamura, and R Cerezo-Mota, 2012: Mid-century warming in the Los Angeles region: Part I of the "Climate Change in the Los Angeles Region" project. Available at http://c-change.la/pdf/LARC-web.pdf

Hara, M., T. Yoshikane, H. Kawase, and F. Kimura, 2008: Estimation of the impact of global warming on snow depth in Japan by the pseudo-global-warming method. Hydrol. Res. Lett., 2, 61–64.

Howat, I. M., and S. Tulaczyk, 2005: Climate sensitivity of spring snowpack in the Sierra Nevada. J. Geophys. Res., 110, F04021, doi:10.1029/2005JF000356

Hughes M., A. Hall, and R.G. Fovell, 2007: Dynamical controls on the diurnal cycle of temperature in complex topography. Clim. Dynam., 29, 277-292,DOI: 10.1007/s00382-007-0239-8.

Hughes M., A. Hall, and R.G. Fovell, 2009: Blocking in areas of complex topography, and its influence on rainfall distribution. J. Atmos. Sci., 66, 508-518, DOI: 10.1175/2008JAS2689.1

Judson, A. and N. Doesken, 2000: Density of Freshly Fallen Snow in the Central Rocky Mountains. Bull. Amer. Meteor. Soc., 81, 1577–1587.

Kapnick S, Hall A, 2010: Observed climate-snowpack relationships in California and their implications for the future. J. Clim. 23: 3446-3456, DOI:10.1175/2010JCLI203.1

Kapnick, S. and Hall A., 2012: Causes of recent changes in western North American snowpack. Clim. Dyn. 38, 1885-1899, doi: 10.1007/s00382-011-1089-y

Kawase, H., T. Yoshikane, M. Hara, F. Kimura, T. Yasunari, B. Ailikun, H. Ueda, and T. Inoue, 2009: Intermodel variability of future changes in the Baiu rainband estimated by the pseudo global warming downscaling method. J. Geophys. Res., 114, D24110, doi:10.1029/2009JD011803

Kay, J. E., 2006: Snow density observations in the Washington Cascades. Proceedings of the 74th Western Snow Conference, Las Cruces, NM, 12 pp.

Kim, J., T. Kim, R. W. Arritt, and N. L. Miller, 2002: Impacts of increased atmospheric CO2 on the hydroclimate of the western United States. J. Clim., 15, 1926–1942.

Knowles, N., and D. R. Cayan, 2002: Potential effects of global warming on the Sacramento/San Joaquin watershed and the San Francisco estuary. Geophys. Res. Lett., 29(18), 1891, doi:10.1029/2001GL014339.

Leung L.R., and S.J. Ghan, 1999: Pacific Northwest Sensitivity Simulated by a Regional Climate Model Driven by a GCM. Part II: 2XCO2 Simulations, J. Climate, 12, 2031–2053.

Leung L.R., Y. Qian, and X. Bian, 2003: Hydroclimate of the western United States based on observations and regional climate simulations of 1981–2000. Part I: seasonal statistics. J. Climate, 16, 1892–1911.

Leung, L R, Y. Qian, X. Bian, W. M. Washington, J. Han, and J. O. Roads, 2004: Mid-century ensemble regional climate change scenarios for the western United States. Climatic Change, 62, 75–113.

Lobell, D. B., and G. P. Asner, 2003: Climate and management contributions to recent trends in U.S. agricultural yields. Science, 299, 1032.

Lundquist, J.D., D.R. Cayan, 2007: Surface temperature patterns in complex terrain: Daily variations and long-term change in the central Sierra Nevada, California. J. Geophys. Res., 112, D11124.

Meehl, G.A., et al., 2007: Global climate projections. In Climate Change 2007: The Physical Science Basis. Contribution of Working Group I to the Fourth Assessment Report of the Intergovernmental Panel on Climate Change [Solomon, S., D. Qin, M. Manning, Z. Chen, M. Marquis, K.B. Averyt, M. Tignor and H.L. Miller (eds.)] Cambridge University Press, Cambridge, United Kingdom, and New York, NY, USA.

Meinshausen, M., S. J. Smith, K. V. Calvin, J. S. Daniel, M. Kainuma, J.-F. Lamarque, K. Matsumoto, S. A. Montzka, S. C. B. Raper, K. Riahi, A. M. Thomson, G. J. M. Velders and D. van Vuuren, 2011: The RCP greenhouse gas concentrations and their extension from 1765 to 2300. Climatic Change (Special Issue), DOI:10.1007/s10584

Meyer, Jonathan D. D., Jiming Jin, Shih-Yu Wang, 2012: Systematic patterns of the inconsistency between snow water equivalent and accumulated precipitation as reported by the Snowpack Telemetry Network. J. Hydrometeor, 13, 1970–1976. doi: http://dx.doi.org/10.1175/JHM-D-12-066.1

Moss R., M. Babiker, S. Brinkman, E. Calvo, T.R. Carter, J. Edmonds, I. Elgizouli, S. Emori, L. Erda, K. Hibbard, R. Jones, M. Kainuma, J. Kelleher, J.-F. Lamarque, M.R. Manning, B. Matthews, J. Meehl, L. Meyer, J.F.B. Mitchell, N. Nakicenovic, B. O'Neill, R. Pichs, K. Riahi, S.K. Rose, P. Runci, R.J. Stouffer, D.P. van Vuuren, J.P. Weyant , T.J. Wilbanks, J.P. van Ypersele, and M. Zurek, 2008: Towards new scenarios for analysis of emissions, climate change, impacts, and response strategies. IPCC Expert Meeting Report, 19–21 September 2007. Noordwijkerhout, The Netherlands, pp 155.

Mote, P. W., 2003: Trends in SWE in the Pacific Northwest and their climatic causes. Geophysical Research Letters, 30(12), doi: 10.1029/2003GL017258

Mote P., 2006: Climate-driven variability and trends in mountain snowpack in Western North America. J Clim, 19, 6209–6220.

Mote P., A. Hamlet, M. Clark, and D. Lettenmaier, 2005: Declining mountain snowpack in Western North America. Bull Am Meteorol Soc, 86, 39–40.

Pan, L.-L., S.-H. Chen, D. Cayan, M.-Y. Lin, Q. Hart, M.-H. Zhang, Y. Liu, and J. Wang, 2011: Influences of climate change on California and Nevada regions revealed by a high-resolution dynamical downscaling study. Clim. Dynam., 37, 2005–2020.

Pavelsky, T. M., S. Kapnick, and A. Hall, 2011: Accumulation and melt dynamics of snowpack from a multiresolution regional climate model in the central Sierra Nevada, California. J. Geophys. Res., 116, D16115, doi:10.1029/2010JD015479

Pierce, D., and D. Cayan, 2012: The uneven response of different snow measures to human-induced climate warming. J. Climate, doi:10.1175/JCLI-D- 12-00534.1, in press.

Pomeroy, J.W. and E. Brun, 2001: Physical properties of snow. In Snow Ecology: an Interdisciplinary Examination of Snow-covered Ecosystems (eds. H.G. Jones, J.W. Pomeroy, D.A. Walker and R.W. Hoham). Cambridge University Press, Cambridge, UK, 45–118.

Qian, Y., S.J. Ghan, and L.R. Leung, 2009: Downscaling hydroclimatic changes over the Western U.S. Based on CAM subgrid scheme and WRF regional climate simulations. Int. J. Climatol., 30, 675–693.

Rasmussen, R., and coauthors, 2011: High-resolution coupled climate runoff simulations of seasonal snowfall over Colorado: a process study of current and warmer climate. J. Climate, 24, 3015–3048.

Roebber P.J., S.L. Bruening, D.M. Schultz, and J.V. Cortinas, 2003.: Improving snowfall forecasting by diagnosing snow density. Weather and Forecasting, 18(2), 264–287.

Sato, T., F. Kimura, and A. Kitoh, 2007: Projection of global warming onto regional precipitation over Mongolia using a regional climate model. J. Hydrol., 333, 144–154.

Skamarock W. C., J. B. Klemp, J. Dudhia, D. O. Gill, D. M. Barker, M. G. Duda, X.-Y. Huang, W. Wang, and J. G. Powers, 2008: A description of the Advanced Research WRF Version 3. NCAR Tech. Note NCAR/TN-475+STR, June 2008, 125 pp.

Snyder, M. A., L. C. Sloan, and J. L. Bell, 2004: Modeled regional climate change in the hydrologic regions of California: A CO2 sensitivity study. J. Am. Water Resour. Assoc., 40, 591–601.

Taylor K., R.J. Stouffer, and G.A. Meehl, 2009: A summary of the CMIP5 Experiment Design. http://cmip-pcmdi.llnl.gov/cmip5/docs/Taylor_CMIP5_design.pdf

U.S. Metro Economies – Outlook – Gross Metropolitan Product, and Critical Role of Transportation Infrastructure, 2012: The United States Conference of Mayors and The Council on Metro Economies and the New American City. Global Insight, Inc.

Voldoire, A. and coauthors, 2012: The CNRM-CM5.1 global climate model: description and basic evaluation. Climate Dynamics, 1–31, 10.1007/s00382-011-1259-y.

von Storch, H., E. Zorita and U. Cubasch, 1993: Downscaling of global climate change estimates to regional scales: An application to Iberian rainfall in wintertime. J. Climate, 6,1161–1171.

Wang Y., L.R. Leung, J.L. McGregor, D.K. Lee, W.C. Wang, Y. Ding , and F. Kimura, 2004: Regional climate modeling: progress, challenges, and prospects. J. Meteor. Soc. Japan., 82, 1599–1628.

Watanabe, S. and coauthors, 2011: MIROC-ESM: model description and basic results of CMIP5-20c3m experiments. Geosci. Model Dev. Discuss, 4,1063–1128.

Wilby, R.L., S.P. Charles, E. Zorita, B. Timbal, P. Whetton, L.O. Mearns, 2004: Guidelines for use of climate scenarios developed from statistical downscaling methods: supporting material of the Intergovernmental Panel on Climate Change, Task Group on Data and Scenario Support for Impacts and Climate Analysis, Rotherham.